ADVANCED ENERGY MATERIALS
www.advenergymat.de

Experimental and Theoretical Advances on Single Atom and Atomic Cluster-Decorated Low-Dimensional Platforms towards Superior Electrocatalysts

Tianwei He, Alain R. Puente-Santiago, Shiyu Xia, Md Ariful Ahsan, Guobao Xu,* and Rafael Luque**

The fundamental relationship between structure and properties, which is called "structure-property", plays a vital role in the rational designing of high-performance catalysts for diverse electrocatalytic applications. Low-dimensional (LD) nanomaterials, including 0D, 1D, 2D materials, combined with low-nuclearity metal atoms, ranging from single atoms to subnanometer clusters, are currently emerging as rising star nano-architectures for heterogeneous catalysis due to their well-defined active sites and unbeatable metal utilization efficiencies. In this work, a comprehensive experimental and theoretical review is provided on the recent development of single atom and atomic cluster-decorated LD platforms towards some typical clean energy reactions, such as water-splitting, nitrogen fixation, and carbon dioxide reduction reactions. The upmost attractive structural properties, advanced characterization techniques, and theoretical principles of these low-nuclearity electrocatalysts as well as their applications in key electrochemical energy devices are also elegantly discussed.

1. Introduction

The design of powerful, green, and scalable energy-related nanomaterials is covering a significant part of the current research endeavors in the material science community due to the paramount role of sustainable energy research to switch the modern economy from the fossil fuels and electric/fuels to zero-emissions technologies.[1] For instance, thanks to the upcoming scientific advances, battery-electric trains will reach similar prices compared with those of diesel-electric trains at near-future, thus reducing the environmental impact and making possible a pollutant-free world.[2] Among all the renewable energy technologies, energy conversion has become a central pillar to construct efficient electrochemical devices such as metal-air batteries and different types of fuel cells.[3] Up to now, noble metals (e.g., Pt, Pd, Ag) are still leading the field of electrocatalysis as the benchmark catalysts,[4] but their low abundance in nature and high prices drastically limit their practical applications.[5] Thus, in the last decades, several efforts have been focused on the assembly of alternative electrocatalytic materials to increase catalytic efficiency and maximize atom economy.[6]

Low-nuclearity supported metal electrocatalysts, ranging from single atom catalysts (SACs) to subnanometer clusters supported onto low-dimensional (LD) carbon networks, have been recently gaining an increasing attention for several

T. He
Fritz-Haber-Institut der Max-Planck-Gesellschaft
Faradayweg 4-6, 14195 Berlin, Germany
A. R. Puente-Santiago, M. A. Ahsan
Department of Chemistry
University of Texas at El Paso
500 West University Avenue
El Paso, TX 79968, USA
E-mail: arpuentesan@utep.edu

The ORCID identification number(s) for the author(s) of this article can be found under https://doi.org/10.1002/aenm.202200493.

DOI: 10.1002/aenm.202200493

S. Xia, G. Xu
State Key Laboratory of Electroanalytical Chemistry
Changchun Institute of Applied Chemistry
Chinese Academy of Sciences
Changchun, Jilin 130022, P. R. China
E-mail: guobaoxu@ciac.ac.cn
S. Xia, G. Xu
University of Science and Technology of China
Hefei, Anhui 230026, P. R. China
R. Luque
Department of Organic Chemistry
University of Cordoba
Campus de Rabanales
Edificio Marie Curie (C-3), Ctra Nnal IV-A, Km 396, Cordoba E14014, Spain
E-mail: q62alsor@uco.es
R. Luque
Peoples Friendship University of Russia (RUDN University)
6 Miklukho-Maklaya str
Moscow 117198, Russia

electrocatalytic reactions because of their unique capabilities to generate highly reactive catalytic spots, unbeatable atom utilization efficiencies and impressive electrocatalytic performances.[7–11] Specifically, atomic cluster electrocatalysts (ACEs), which could be formed by two or more atoms, are gaining an unprecedented interest in the scientific community nowadays because of their highly tunable catalytic properties.[12,13] In this regard, tuning the number of atoms of tiny metal clusters, from a single atom to at most a few tens of atoms, can regulate both their geometric and electronic properties as well as their catalytic reactivities with atomic-level precision.[7,14] Most importantly, unlike their metal nanoparticle counterparts, controlling the short-range interactions of single atom and atomic clusters with their nanocarbon platforms represents a powerful tool to tailor the adsorption energy of intermediate catalytic species towards more effective electrocatalytic rates. As a result, a variety of very attractive SACs and ACEs electrocatalysts, which use LD carbon nanomaterials as supporting platforms, have risen as the new frontier of heterogeneous catalysis. Indeed, they are paving the way to understand the electrocatalytic phenomena at the subnanometer level.

The molecular-level engineering of SACs can finely optimize both the electronic structure and intermediate adsorption of intermediates catalytic species via structural and space effects.[15] Moreover, there is an increasing interest in applying SACs in biomedical fields for enzyme-mimic catalysis and disease therapy.[16] Additionally, ACE electrocatalysts provide a unique opportunity to unravel the effects of atom-by-atom interaction and electron confinement in the catalytic pathways of several reactions.[17]

In this Review, we summarize the most innovative ideas on the synthesis of atomic-scale electrocatalysts based on single atoms and subnanometer clusters supported onto LD platforms, thus providing insightful guidelines for the efficient design of the upcoming generation of low-nuclearity electrocatalysts. We address a comprehensible discussion on the structural-catalytic function relationships of the state-of-the-art low-nuclearity electrocatalysts. Additionally, the electrochemical performance of low-nuclearity catalysts as superb active electrodes of water splitting devices, Zn–air-batteries, and fuel cell devices is presented. Most importantly, although some reviews in the field of subnanometer cluster electrocatalysts have been reported, we cover an in-depth understanding of the electrocatalytic behavior of these nanoarchitectures for a wide range of catalytic reactions such as water splitting, NRR, and CO_2RR using a unique combination of experimental and theoretical arguments.

2. Synthesis of LD Material-Based SACs

2.1. Wet Chemical Strategy

Generally speaking, the synthesis of SACs involves wet chemical synthesis with many strategies, such as hydrothermal/solvothermal method, impregnation method, ion exchange strategy, etc. The wet chemical synthesis method is usually mild in reaction conditions and simple in operation, thus it has little influence on the support in the synthesis process. Here, several synthetic methods are briefly introduced.

2.1.1. Solvothermal/Hydrothermal Synthesis Strategy

Solvothermal/hydrothermal method is a typical and practical wet-chemical synthesis strategy. The aim of one-step synthesis can be achieved by simply mixing the metal precursor, the treated support and reductant in the autoclave, simplifying the experiment, thus allowing the synthesis of SACs supported on different carriers including metallic supports (e.g., stainless steel or zirconium),[18] N,S-codoped graphene oxide,[19] metallic oxide (such as CeO_2 nanowires),[20] etc. Liu's group[21] synthesized a single cobalt atom catalyst supported on 2D Bi_3O_4Br nanosheets by one-step solvothermal method. Bismuth, cobalt metal precursors, and polyvinylpyrrolidone were dispersed in mannitol, and NaBr dissolved in mannitol was added while stirring, the suspension was transferred to an autoclave for reaction in an oven, Co atoms replaced Bi atoms in the lattice to achieve cobalt loading. Moreover, precious metal catalysts supported on manganese dioxide have also been studied. There are many defects such as manganese and oxygen vacancies, abundant surface hydroxyl groups, and interlayer cations in the structure of MnO_2, which often show extremely high activity.[22] Therefore, SACs supported by MnO_2, such as, Pt-MnO_2 nanosheets (2D),[22] Ag-MnO_2 nanowires (1D),[23] and Pd-MnO_2 nanowire (1D)[24] SACs, have been widely studied (**Figure 1**A–C). Zhang's group[22] anchored single-atom Pt on ultrathin MnO_2 nanosheets by a one-pot hydrothermal method.

2.1.2. Impregnation Strategy

The impregnation method is one of the most common methods for preparing SAC, which involves the immersion of the support into the catalyst precursor solution, causing the metal atoms adsorption on supports, and the subsequent evaporation, drying, calcination and reduction. Thus, the method is generally divided into two parts, one is the preparation of the carrier, and the other is the loading of metal atoms. Therefore, this method can conveniently load the same metal on different supports and compare the differences in performance caused by the supports. Zhang et al.[25] anchored Pt single atom on two kinds of supports, RuO_2 and VXC-72 respectively, by the method of impregnation-adsorption, and compared the catalytic performance of the two kinds of catalysts. Lu et al.[26] also used this method to explore the influence of carrier morphology and local coordination environment of isolated metal atoms caused by heteroatom species doped on the carrier surface on the performance. This characteristic endows impregnation method with the function of studying the role of carrier in catalyst. Xu et al.[27] prepared Ru SACs anchored on nitrogen-doped reduced graphene (Ru-N/rGO) by this method. The introduction of nitrogen heteroatoms changed the surrounding coordination environment and produced coordination unsaturated sites. The nitrogen heteroatom on rGO carrier is used as a "trap" to capture Ru^{3+}, which provides a favorable anchor point for monatomic Ru (Figure 1D). In addition, this method is also used in the preparation of rare earth metal catalysts. Xie's group[28] used 2D TiO_2 nanosheets with oxygen vacancies to anchor rare earth metals, La and Er, and synthesized rare earth metal SACs.

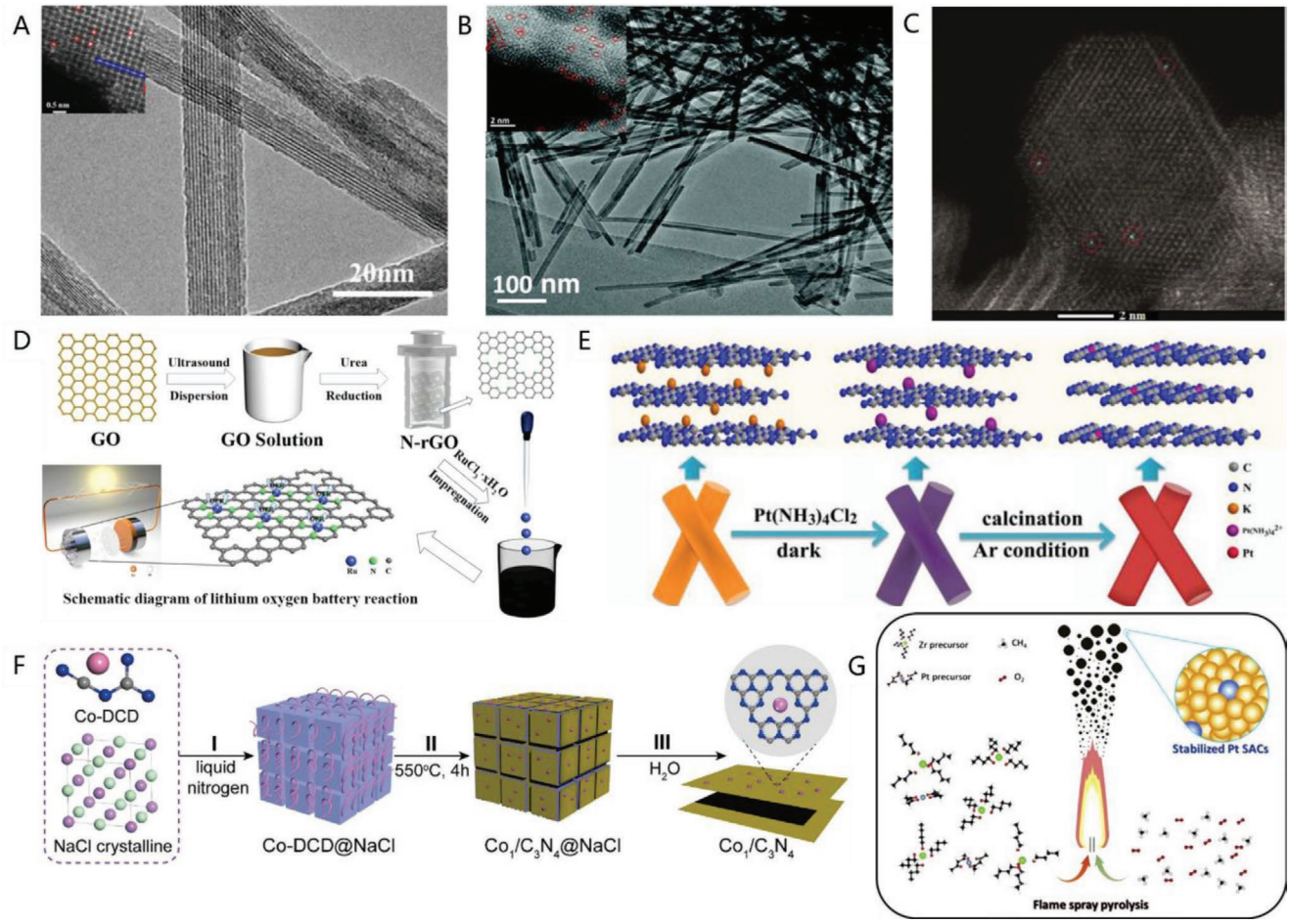

Figure 1. A–C) Electron microscope images of A) Ag-MnO_2 nanowires (Adapted with permission.[23] Copyright 2019, Elsevier), B) Pd—MnO_2 nanowire (Adapted with permission.[24] Copyright 2019, Royal Chemistry Society) SACs and C) Pt—MnO_2 nanosheets (Adapted with permission.[22] Copyright 2019, Elsevier). D) Schematic illustration of the fabrication procedure of the Ru-N/rGO and its HAADF-STEM images. Adapted with permission.[27] Copyright 2021, Elsevier. E) Schematic illustration of the synthetic process of Pt/g-C_3N_4 SACs and its HAADF-STEM images. Adapted with permission.[30] Copyright 2020, Elsevier. F) Schematic illustration of the synthetic process of Co_1/C_3N_4 nanosheets. Adapted with permission.[32] Copyright 2020, Elsevier. G) Schematic diagram of the synthetic process of Pt SACs via flame spray pyrolysis. Adapted with permission.[33] Copyright 2021, Elsevier.

2.1.3. Ion Exchange Strategy

Ion exchange strategy is a new wet chemical synthesis method, which simplifies the steps and can usually operate at a lower temperature compared with traditional wet impregnation method which requires precise control of pH and temperature.[29] It is universal and promising for the synthesis of various metal catalysts. Zhang's group[30] used the carbon nitride embedded with potassium ions (g-C_3N_4-K) as the initial precursor, stirred for one day at room temperature, and mixed with platinum precursor thoroughly to achieve the purpose of ion exchange between potassium ion and platinum ion, and then calcined to obtain SA-Pt/g-C_3N_4 catalyst. This interlayer structure endows a single Pt atom with an ultra-high load, and the limited interlayer environment makes the Pt charge density delocalized, and the Pt atom limited by interlayer space is more active than the Pt atom located in the surface layer (Figure 1E). Kim's group[31] confirmed the universality of the method (Cu, Fe, Co, Mn SACs). The researchers prepared calcium alginate hydrogel (AG–Ca) by the reaction of natural nontoxic polysaccharide-sodium alginate and calcium chloride. After acidification, AG–H was obtained. Then, different metal precursors were introduced for ion exchange reaction, and the catalysts were obtained following thermal annealing.

2.2. Pyrolysis Strategy

Pyrolysis is the most commonly used synthetic method of SACs, which usually operates at high temperature (usually at 600–1000 °C, a few below 600 °C[32]), and this high temperature is also conducive to the formation of surface defects of the support. Carbon-based materials of various dimensions (0D–2D) are widely used as supports.[34–36] The introduction of heteroatom dopant or functional groups can enrich the available anchoring points of metal atoms and enhance the anchoring ability by forming M—N_x part, which requires high-temperature heat treatment.[37–39] Liu and coworkers[32] prepared Co_1/C_3N_4 nanosheets by using the crystal-assisted confinement pyrolysis method, dicyandiamide (DCD) was used as the nitrogen and

carbon source of 2D carrier carbon nitride (C_3N_4), and sodium chloride was used as the microcrystalline template, which was mixed with Co precursor, and then freeze-dried and pyrolyzed (Figure 1F). Besides, the research of using biomolecules containing both carbon and nitrogen as the carrier source of SACs has also been carried out, such as guanosine.[40] Moreover, the loading on metal oxides can be realized through a special flame spray pyrolysis process. Yan et al.[33] carried out the preparation of thermally stable metal oxide (Al_2O_3, SiO_2, TiO_2, and ZrO_2) supported single Pt catalyst by flame spray pyrolysis, which favored the formation of tetragonal-monoclinic phase of ZrO_2 with improved redox property, thus improving the catalytic activity (Figure 1G).

2.3. Electrochemical Synthesis Strategy

It is a new synthetic strategy to drive the deposition of a single metal atom on the surface of LD nanomaterials by electric field. Different from carbon-based support catalysts usually produced by pyrolysis methods, various types of supported catalysts can be prepared by electrochemical methods, and catalysts supported by different supports can be easily realized by employing different substrate electrodes. Various methods based on electrochemical synthesis have been developed, such as electroplating,[41] electrospinning,[42] and arc discharge.[43] Researchers[41] have realized the deposition of single Pt, Au, and Pd on 2D MoS_2 by electroplating, which is attributed to the fact that noble metal atoms can be dissolved when the anode voltage is higher than 1.1 V (versus RHE),[44] while the Mo- and S-vacancies in MoS_2 have a strong tendency to absorb foreign atoms for capture purposes (**Figure 2**A). Chen et al.[45] developed a cobalt single atom-intercalated molybdenum disulfide catalyst (Co_1-in-MoS_2) with vertical structure by electrochemical cointercalation method. Co precursor, cobalt phthalocyanine (CoPc), was encapsulated in MoS_2 matrix by electrochemical co-intercalation method using as-grown MoS_2 array on carbon paper as working electrode, and SACs were obtained after thermal annealing (Figure 2B). Arc discharge method is distinctly different from the conventional electrochemical technology, which uses the high energy generated by the discharge process to provide a high-temperature environment to realize the synthesis of SACs. Kim's group used this method to realize the loading of Co, Ni, Mn, and other single metal atoms on carbon-based materials.[43] The metal precursor (chloride) was dissolved in acetone and then mixed with carbon powder to make the filling material of anode parts, and the chamber gas also participated in the reaction and evaporated after arc discharge to form SACs. This study revealed that nitrogen atoms in buffer gases and chlorine atoms as precursor molecules

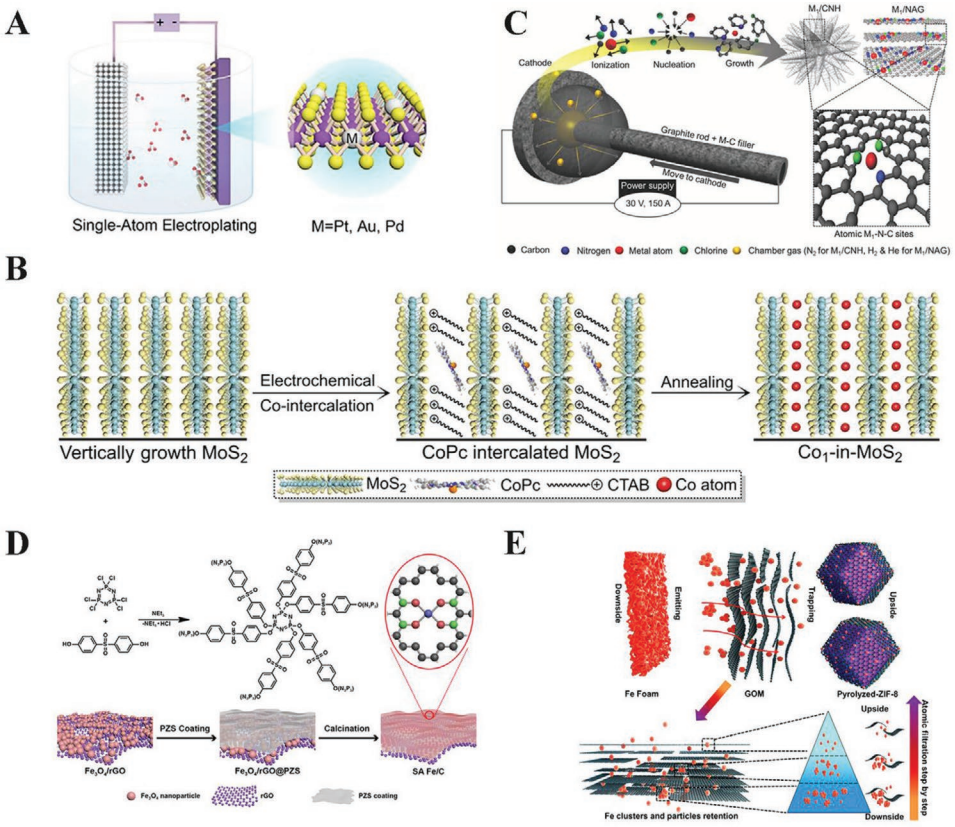

Figure 2. A) Schematic illustration of the synthetic process of Pt, Au, and Pd SACs via electroplating synthesis. Adapted with permission.[41] Copyright 2019, American Chemical Society. B) Schematic illustration of the synthetic process of Co_1-in-MoS_2 via electrochemical co-intercalation method. Adapted with permission.[45] Copyright 2020, Wiley. C) Synthetic schematic diagram of Co, Ni, Mn SACs via arc discharge method. Adapted with permission.[43] Copyright 2021, Wiley. D,E) SACs synthesized from nanoparticles. Adapted with permission.[46] Copyright 2021, Wiley. E) Bulk metals via solid-diffusion strategy. Adapted with permission.[47] Copyright 2020, American Chemical Society.

played crucial roles in dispersing and stabilizing metal atoms during nanocarbon synthesis (Figure 2C).

2.4. Solid-Diffusion Strategy

Solid diffusion strategy is a top-down strategy, which can be divided into two types, one is the migration from nanoparticles to form single atoms,[46,48,49] and the other is the migration from bulk metals to form single atoms.[47,50] Song et al.[46] reported the preparation of oxygen coordination metal monatomic catalysts by pyrolysis of the metal oxides. The metal oxide nanoparticles were loaded on graphene nanosheets (M_xO_y/rGO) for capturing metal ions and coated with highly crosslinked poly (cyclotriphosphazene-co-4,4′-sulfonyl diphenol) (M_xO_y/rGO@PZS), which were pyrolyzed at high temperature to obtain corresponding SACs (Fe, Co, Ni, Mn) (Figure 2D). Single atoms can be prepared not only from metal oxides but also from metal nanoparticles. Li's group[49] prepared Ag SACs supported by MnO_2 by thermal diffusion of Ag nanoparticles, that is, Ag NP/MnO_2 to Ag SACs/MnO_2. The researchers used various techniques to explore the mechanism that the Ag nanoparticles collided strongly with the substrate, which caused the surface reconstruction of MnO_2, and the Ag nanoparticle size gradually decreased with the increase of temperature until it disappeared from the surface of manganese dioxide substrate.

The migration from bulk metals has also been reported. Graphene oxide thin films (GOMs) are stacked sheets of graphene oxide, which can screen molecules and ions in aqueous solution, thus GOMs are expected to become an "atomic sieve".[47] Wu's group[47] put forward a unique idea for preparing SACs. They elaborately modulated the layer numbers of the GOMs and their interlayer spacing (comparable to or smaller than the metal atoms), and used them to exclude the diffusion of large metal species (clusters and particles), thus preparing Fe SACs. Fe foam is used as the Fe source, from which Fe atoms are thermally released at 1000 °C. GOMs only allow the atomic Fe species to diffuse through the membrane, and metal–organic framework compound, ZIF-8, is used as a carbon carrier to capture the separated iron atoms (Figure 2e).

2.5. Others

Based on the various synthesis strategies proposed above, the reduction or decomposition of metal precursor can be driven by the input energy.[51] Therefore, other ways that can provide energy have been derived for the synthesis of SACs. For example, SACs can be synthesized by molten metal salt,[52] plasma-assisted method,[53] and other methods. A synthetic method based on molten metal salt is reported. Li et al.[52] synthesized transition metal (TM) catalyst (Co, Cu) supported on Ti_2AlN MAX ceramics. The molten $CoCl_2$ (or $CuCl_2$) not only etch the Al layer of Ti_2AlN and produce 2D layered MXene, but also etch some Ti atoms and produce Ti vacancy defects which can anchor Co (or Cu) atoms. These processes were accomplished in one step using the molten TM salts, thus avoiding complicated pretreatment. In addition, the synthesis of SACs can also be realized by atomic isolation strategy.[54] Cheng et al.[54] synthesized a series of single-atom Fe catalysts with similar 1D core–shell structures, namely CNF-900 @ Fe—N—C, CNF-1100 @ Fe—N—C, or carbon nanotube (CNT)@ Fe—N—C via this method. The method first involves a simultaneous adsorption process of Zn and Fe, and then removes Zn through high-temperature treatment to obtain Fe SACs.

3. Synthesis of LD Material-Based Sub-Nano Atomic Clusters (SNACs)

3.1. Wet-Chemical Strategy

The conversion between SACs with lower loading and ACs with higher loading can usually be realized by controlling the conditions affecting the metal load amount in wet chemical methods, including pH, reaction temperature, and precursor concentration, or adding additional post-treatment steps (such as pickling).[55–57] In addition, the synthesis of multi metal clusters can also be acquired by simultaneously introducing several metals. Obviously, the wet chemical methods can be divided into many synthetic routes, including chemical reduction, co-precipitation, electrochemical, solvothermal/hydrothermal reaction process, and so on. Here we make a brief introduction.

Chen's group[58] constructed Pd ACEs by chemical reduction, and Pd atoms were confined in the pores of porous 1D CeO_2 nanorods through Pd—O bonds. In addition, cluster means the existence of multiple atoms, so clusters composed of different metal atoms are also an important part of ACEs (**Figure 3**A). Li's group[59] introduced trithiol-terminated poly(methacrylic acid) as ligand to assist reduction to prepare three kinds of Pt-M(Au, Cu, Pd)/TiO_2 ACEs. The polymer first acted with two metal precursors, and then co-reduced under the action of reducing agent to obtain catalysts with different compositions (Figure 3B). The coprecipitation method is also a powerful means to prepare multi-metal (or monometallic) sub-nano clusters, such as Cu-FeOOH/g-C_3N_4 nanosheet and Rh/$Fe(OH)_x$.[60,61] For the electrochemical process, Hui's group[62] prepare uniform ultrafine sub-nanometer Pt clusters anchored on defect-rich NiFe LDHs sheets in an electrolyte containing Ni^{2+}, Zn^{2+}, Fe^{2+}, Pt^{4+} by a facile electrodeposition method (Figure 3C). Additionally, Gao's group[63] also used a simple one-pot hydrothermal synthesis strategy to prepare Co_3O_4/TiO_2 ACEs (Figure 3D).

3.2. Impregnation Strategy

Cost-effective and common impregnation strategies are also used to synthesize sub-nano cluster catalysts. The aforementioned impregnation method involves the interaction between the carrier and the metal, and its strength will affect the catalyst loading, stability, and dispersion uniformity. He's group[64] used the litchi pericarp as carbon source, which is etched by K_2CO_3 to obtain a carrier with double limitation of carbon defect and micropore structure. Then different metal clusters were prepared by immersion in the solution containing M^{n+} (Cu, Fe, Co, Ni) and calcination. In addition, Yu's group[65] prepared two kinds of self-supporting MFI zeolite nanosheets (SP-S-1

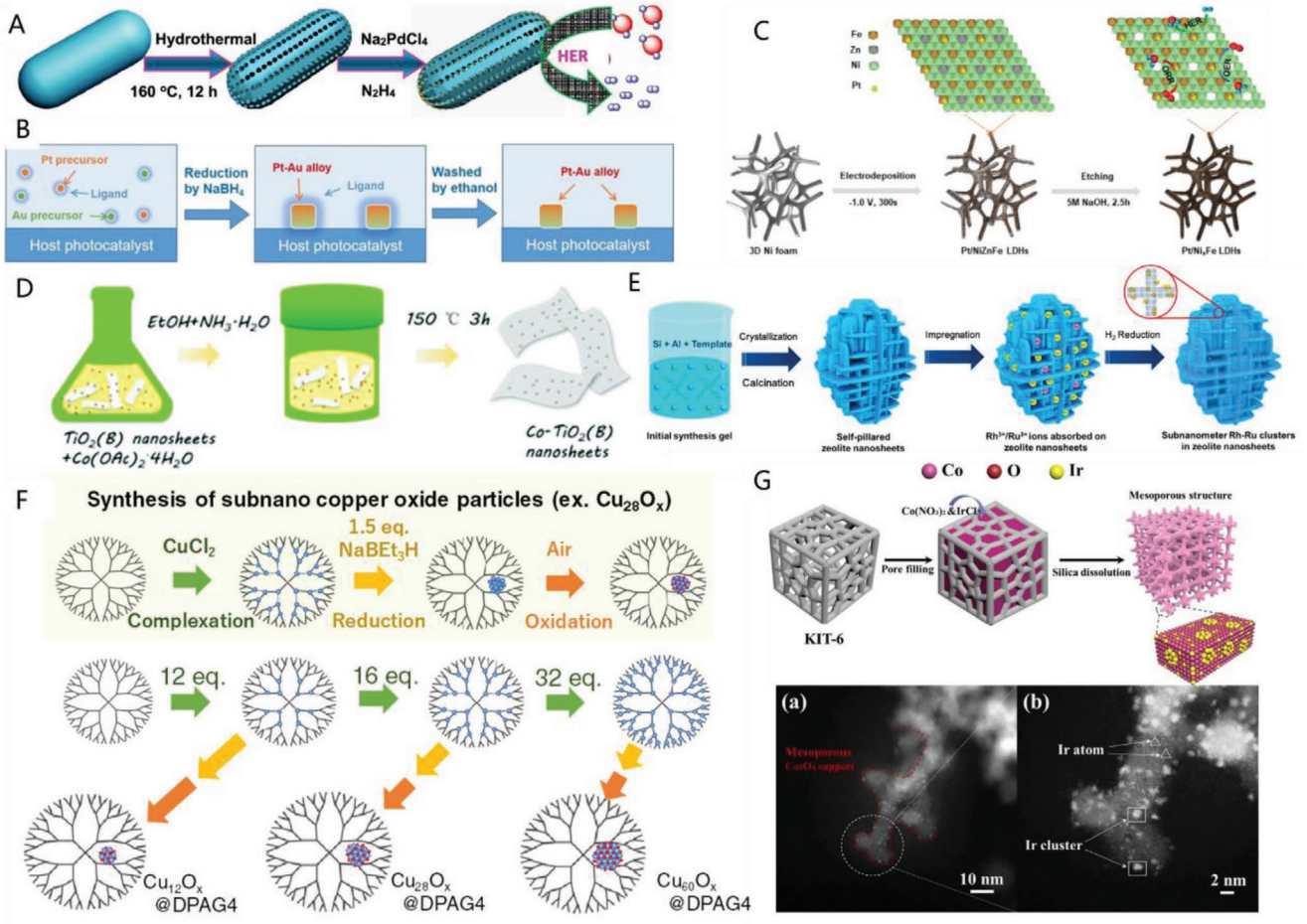

Figure 3. A–D) Wet-chemical strategy. A) Schematic of the fabrication of Pd/CeO_2 nanorods. Adapted with permission.[58] Copyright 2019, American Chemical Society. B) Schematic of the fabrication of Pt—M(Au, Cu, Pd)/TiO_2. Adapted with permission.[59] Copyright 2019, Wiley. C) Schematic illustration of Pt/NiFe LDHs. Adapted with permission.[62] Copyright 2021, American Chemical Society. D) Synthetic schematic diagram of Co_3O_4/TiO_2 ACEs. Adapted with permission.[63] Copyright 2018, Royal Chemistry Society. E) Synthetic schematic diagram of Ru or/and Rh ACEs via impregnation strategy. Adapted with permission.[65] Copyright 2021, American Chemical Society. F,G) Template-assisted strategy. Synthetic schematic diagram of Cu_nO_x (n = 12, 28, 60) ACEs. Adapted with permission.[67] Copyright 2020, American Chemical Society. G) Synthetic schematic diagram of Ir/Co_3O_4 ACEs and corresponding HAADF-STEM image. Adapted with permission.[68] Copyright 2019, Wiley.

and SP-ZSM-5) which are different from traditional zeolites as carriers. They have significantly increased specific surface area and abundant Si-OH defects, which facilitate the immobilization and dispersion of metals. Then different monometallic and bimetallic cluster (Ru or/and Rh) catalysts are loaded by impregnation (Figure 3E). In addition to optimizing the carrier, introducing some metals in the impregnation process can also improve the dispersibility of clusters. For example, Ma's group[66] introduced different amounts of tin as promoters to control the dispersion degree of Pt on the support during impregnation, and fabricated fully exposed Pt_3 clusters on the defective nanodiamond@graphene, in which the dispersed Sn atoms play a role in geometric partitioning.

3.3. Template-Assisted Strategy

Template-based technology is equivalent to adopting the "nano-reactor" mode, which limits the reaction in a certain space, avoiding the aggregation of metal particles and facilitating size control.[69,70] The most widely used template is dendrimer, such as dendritic tetraphenylmethane (DPAG4),[67] mono(2-pyridyl)-triphenylmethane, phenylazomethine.[71] Yamamoto's group[67] controllably prepared a series of Cu_nO_x (n = 12, 28, 60) ACEs with different sizes via simply adjusting the ratio of metal precursor to DPAG4 template. The stability of copper oxide clusters is solved by the enhanced ionicity of Cu—O bond with decreasing size (Figure 3F). Besides, other types also have been developed. Luo's group[72] designed a route of single micelle-directed interfacial assembly using poly(ethylene oxide)-block-polystyrene as template, which realized in situ formation of manganous oxide (MnO) ACEs and the cross-linking of dopamine (carbon precursor) to polydopamine. It simplified the complicated post-treatment process. Meng's group[68] also used KIT-6 (a form of silica) as a template to construct Ir ACEs supported on mesoporous Co_3O_4. In the process of synthesis, KIT-6 template not only plays an important role in the formation of

Co_3O_4 mesoporous structure, but also effectively inhibits the aggregation of Ir species (Figure 3G).

3.4. Photo-Assisted Strategy

Light-assisted strategy, as a mild synthesis method, can synthesize ultra-small-sized metal catalysts by simply adjusting the light irradiation time, metal precursor types, pH, and other conditions without reducing agent, and at the same time controlling the size and valence state.[73–77] Gao's group[75] developed a convenient short-time (less than 5 min) photo-deposition strategy, in which three kinds of sub-nanometer high-density isolated TM clusters, including Fe, Co, and Ni, were loaded on ultrathin TiO_2 nanosheets, and the sizes and performance of clusters can be regulated by irradiation time(**Figure 4**A). There is no doubt that the existence of defects on the support provides the possibility for the anchoring of metal atoms. Zhu et al.[78] obtained a special structure of coexistence of Ag and AgCl ACEs by photo-induced reduction of Ag^+ adsorbed on the surface of defective $Bi_{12}O_{17}C_{l2}$ nanosheets (BOC-D). Unsaturated Cl atoms due to the existence of vacancies (V_{Bi} and V_{Bi-O}) on BOC-D nanosheets can strongly interact with Ag, resulting in Ag embedded in BOC-D lattice and partially replacing V_{Bi} and V_{Bi-O}. While fewer Cl atoms limit the number of AgCl ACEs formed, a few AgCl SNACs will decompose under continuous irradiation forming Ag ACEs (Figure 4B).

3.5. Others

Apart from the above-mentioned strategies, other methods including freeze drying-reduction[81] and cage-confinement pyrolysis[82] have been exploited. Sub-nano FeO_x clusters anchored on ultra-thin amorphous Al_2O_3 nanosheets rich in defects and dangling bonds were prepared by freeze-drying–reduction method, which is similar to impregnation method. It replaces the immersion process of the carrier in the solution containing the metal precursor with the process of freeze-drying after mixing the two, thus avoiding the hydrolysis of the Fe precursor effectively.[81] Apart from this, researchers also developed the preparation of ACEs via redox reaction between carrier and metal precursor without additional reducing agent, that is, substrate-enhanced electroless deposition (SEED). This also implies a potential limitation, that is, the reaction can only be carried out when the redox potential of the target metal ions is higher than that of the substrate. Dai et al.[83] first reported this phenomenon in 2002. His group[79] reported Pt/defective graphene (DG) SNACs through the redox reaction between $[PtCl_4]^{2-}$ and DG recently (Figure 4C). In addition to

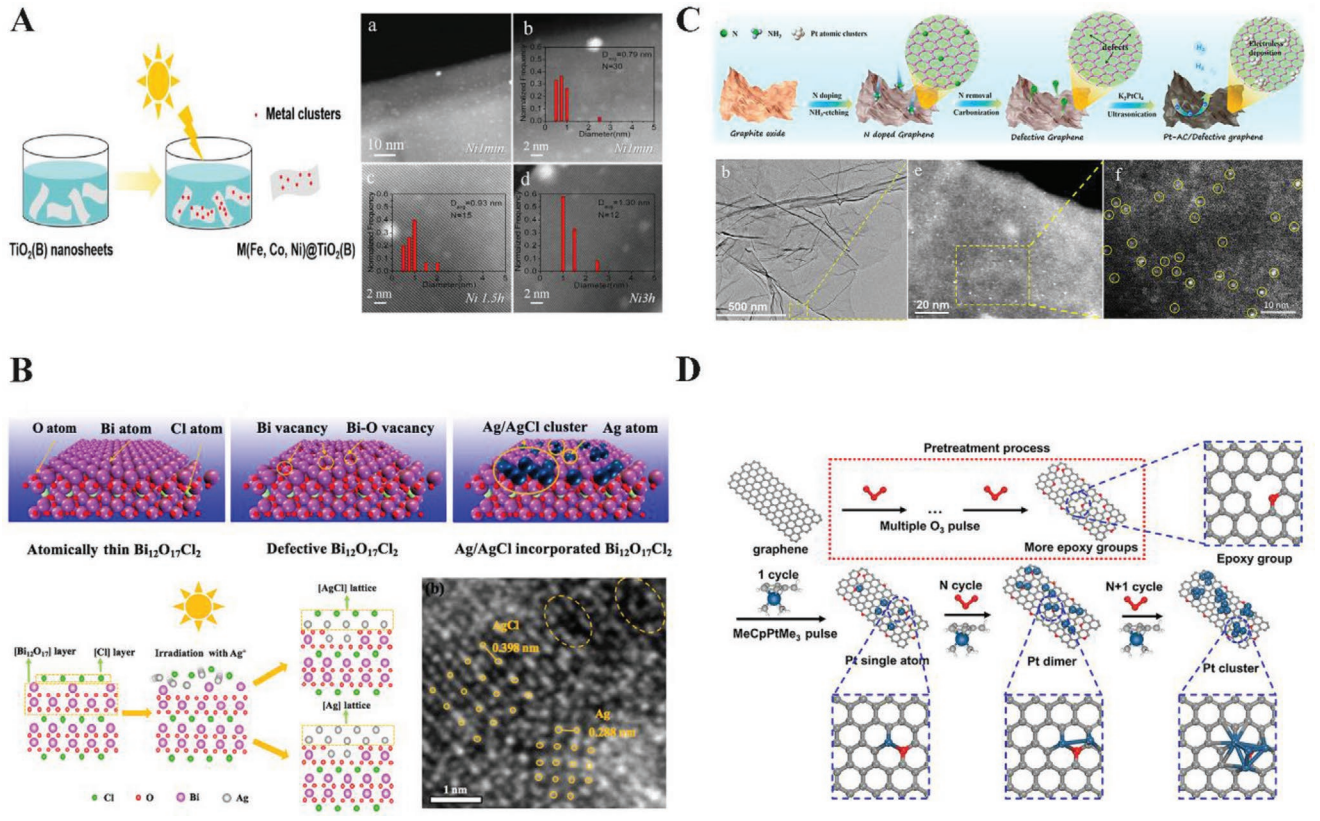

Figure 4. A,B) Photo-assisted strategy. A) Synthetic schematic diagram of Fe, Co, Ni/TiO_2 nanosheets, and Ni/TiO_2 nanosheets under different irradiation time. Adapted with permission.[75] Copyright 2020, Elsevier. B) Ag/AgCl-BOC-D nanosheets, formation mechanism of Ag/AgCl ACEs, and corresponding HAADF-STEM image. Adapted with permission.[78] Copyright 2021, American Chemical Society. C) Synthetic schematic diagram of Pt/DG ACEs and corresponding HAADF-STEM image via SEED. Adapted with permission.[79] Copyright 2020, American Chemical Society. D) Synthetic schematic diagram of Pt ACEs via ALD. Adapted with permission.[80] Copyright 2021, American Chemical Society.

Table 1. Representative catalysts and their applications.

Catalysts	Synthetic strategy		Representative catalysts	Application	Ref.
SACs	Wet chemical strategy	Solvothermal/hydrothermal strategy	Ag-MnO_2	ORR/OER Zn–air battery	[23]
		Impregnation strategy	Ru-N/rGO	ORR/OER Li—O_2 battery	[27]
		Ion exchange strategy	SA-Pt/g-C_3N_4	HER	[30]
	Pyrolysis	Pyrolysis	Fe-N_x-C nanosheets	ORR	[40]
		Flame spray pyrolysis	Pt SACs		[33]
	Electrochemical synthesis	Electroplating	Pt, Au, and Pd SACs	HER	[41]
		Electrochemical co-intercalation method	Co_1-in-MoS_2		[45]
		Discharge method	Fe, Co, Ni, Mn SACs	ORR	[43]
	Solid-diffusion strategy	From nanoparticles	Ag SACs/MnO_2	CO_2 RR	[49]
		From bulk metals	Fe SACs.	ORR	[47]
ACEs	Wet-chemical strategy	Chemical reduction	Pd clusters @CeO_2	HER	[58]
		Electrochemical	Pt clusters/NiFe LDHs	HER/OER/ORR Na–air battery	[62]
		Solvothermal/hydrothermal	Co_3O_4—TiO_2 nanosheets	HER	[63]
	Impregnation strategy		Ru (or/and Rh) clusters/MFI zeolite nanosheets		[65]
	Template-assisted strategy		Ir—Co_3O_4 clusters	OER	[68]
	Photo-assisted strategy		Ag/AgCl-BOC-D clusters	CO_2RR	[78]
	Others	SEED	Pt clusters/DG	HER	[79]
		ALD	Pt/graphene		[80]

the chemical synthesis-based processes, physical processes are also widely used. For example, Qin's group[80] prepared Pt SNACs by atomic layer deposition with graphene rich in epoxy pretreated by multiple O_3 pulses as carrier (Figure 4D). Finally, we summarized various synthesis strategies of SACs and ACEs based on LD materials in **Table 1**.

4. Advanced Characterization Techniques

Low-nuclearity electrocatalysts have been extensively investigated using a framework of experimental and theoretical techniques.[87,88] Among them, high-resolution scanning tunneling microscopy and high angle annular dark-field scanning transmission electron microscopy (HAADF-STEM) are emerging as powerful strategies to elucidate the atomic morphology of atomic catalysts. X-ray absorption spectroscopy (XAS), Fourier-transform infrared spectroscopy (FTIR), X-ray photoelectron spectroscopy (XPS), energy-dispersive X-ray spectroscopy (EDX), electron energy loss spectroscopy (EELS) and surface enhanced Raman spectroscopy (SERS have provided insightful evidence for the existence of low-nuclearity electrocatalysts. In addition, DFT calculations have brought unprecedented breakthroughs towards the discovery of new catalytic reaction mechanisms and catalytically active species.[89,90]

Importantly, the development of in situ characterization methods have been crucial to determine the structure–function relationships of SACs and ACEs in a myriad of electrocatalytic reactions, thus enabling the possibility to track the reaction mechanism as a function of the potential applied and revealing the dynamic evolution of both composition and structure in the surface electrocatalyst under experimental conditions.[91–93]

5. Structural Properties of SACs and ACEs Supported on LD Nanomaterials

5.1. SACs onto 0D, 1D, and 2D Platforms: Structural Properties

SACs with atomically dispersed metal atoms as active sites and carbon nanonetworks as suitable supports have sparked remarkable attention in the field of catalysis.[1,94] In comparison to traditional electrocatalysts, SACs exhibit maximum metal utilization efficiency and low metal consumption, thus facilitating many electrocatalytic processes at the atomic scale. Notably, it is feasible to take advantage of their atomic active sites and tunable coordination environments to design highly selective electrocatalytic nanosystems.

LD carbon-based nanomaterials, such as nanosheets (2D), nanoribbons (1D), and nanodots (0D), have been widely used as supporting substrates of atomic metallic-based catalysts because of their fascinating structural properties such as high surface area and superior electrical conductivities. Carbon nanomaterials with different dimensions have usually shown different mass-transport abilities, which represent a key factor to finely tailor the energetic states of many catalytic intermediates.[95,96] Additionally, LD nanocarbon networks can easily promote sufficient atomic active sites by effectively dispersing metals, thus maximizing the efficiency of several interfacial electrocatalytic processes.[97]

Chang and colleagues established an original coordination adsorption approach for the synthesis of monodispersed Fe single atoms attached on nitrogen anchoring sites of nitrogen-doped graphene quantum dots (N-GQDs) to form $Fe(NO)_2$-N-GQDs as compelling OER electrocatalysts.[84] First, the graphite powder was deeply exfoliated by $PyBr_3$ to obtain a colloidal suspension of graphene layers. Subsequently, N-GQDs were synthesized from graphene layers using a hydrothermal method. The resulting N-GQDs and the precursor $Fe(CO)_2(NO)_2$ were mixed to form $Fe(NO)_2$-N-GQDs (**Figure 5**A). XPS revealed insightful details about the structure of the atomic Fe catalyst. Particularly, the coordination of atomic Fe to the N-GQD network was confirmed by the Fe-N peak at 399 eV of the N 1s core-level (Figure 5B). Interestingly, the improved η_{10} value of the $Fe(NO)_2$-N-GQDs compared with those of their precursor species (Figure 5C) was attributed to the changes in both the surface structure and electronic properties of the N-decorated GCDs upon the attachment of the Fe atomic sites. These findings open an unexplored new synthetic route towards the construction of SACs on 0D nanocarbon surfaces.

1D nanomaterials, such as nanorods (NR), nanotube (NT), nanowire (NW), and nanofiber (NF), have attracted significant efforts in the field of electrocatalysis due to their intrinsic advantages as nanoplatforms of atomically distributed metals such as much higher specific surface area as well as better mass transport properties than 0D-nanostructures.[98,99] Among the most exciting examples, Yi Cheng and coworkers have synthesized a new class of high metal loading CO_2RR SACs from atomically distributed TMs in nitrogen-doped CNTs (MSA-N-CNTs, where M = Ni, Co, NiCo, CoFe, and NiPt) using a simple multistep pyrolysis strategy.[85] The atomic distribution of

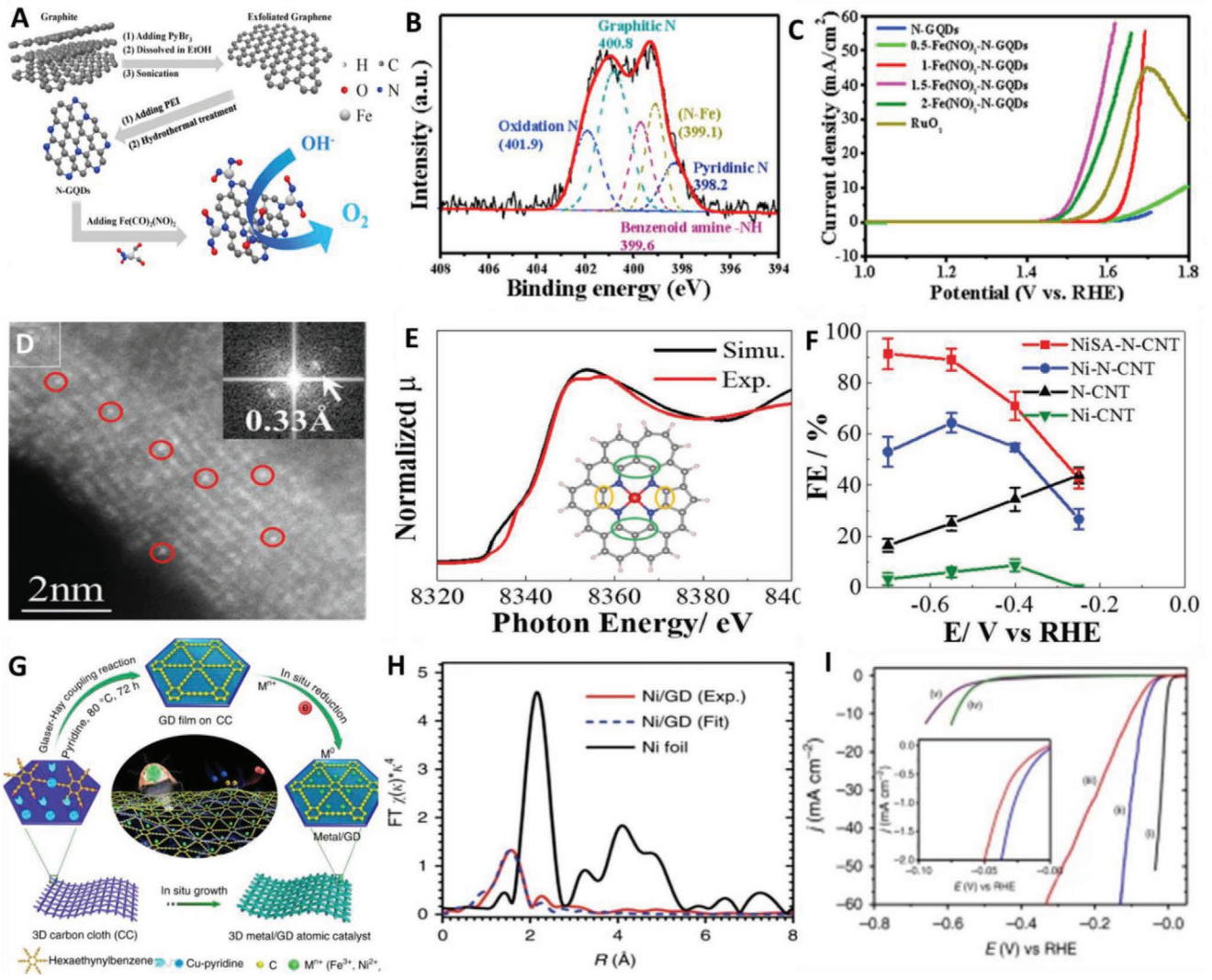

Figure 5. A) Schematic illustration of the synthetic strategy of $Fe(NO)_2$-N-GQDs ACES. B) N 1s XPS band of $Fe(NO)_2$-N-GQDs catalysts. C) OER polarization curves of N-GQDs, $Fe(NO)_2$-N-GQDs, and RuO_2 at a scan rate of 5 mV s^{-1} in a 0.1 M KOH electrolyte. Adapted with permission.[84] Copyright 2021, Elsevier. D) AC-STEM-annular dark-field (ADF) images showing the Ni single atoms located on the walls of a CNT of the NiSA-N-CNTs ACEs. E) Experimental and simulated XANES spectrum of the inserted Ni-core structure. F) FE of CO for NiSA-N-CNTs, Ni-N-CNTs, N-CNTs, and Ni-CNTs at a wide range potential window. Adapted with permission.[85] Copyright 2018, Wiley. G) Schematic diagram for the synthesis of Ni/GD and Fe/GD. H) Ex situ EXAFS spectra of Ni/GD and Ni foil at the Ni K-edge. I) Polarization curves for HER of i) Pt/C, ii) Fe/GD, iii) Ni/GD, iv) GDF, and v) CC. Adapted with permission.[86] Copyright 2018, Nature Publishing Group.

Ni atoms into the CNT platform has been unlocked using aberration-corrected scanning transmission electron microscopy (AC-STEM). The bright dots represent the Ni atomic centers homogenously dispersed into the 1D-network, which is composed of a multiwall structure with an interlayer spacing of 0.33 nm (Figure 5D). Furthermore, the coordination environment of the Ni atomic centers was disentangled by combining STEM and DFT simulations of the X-ray absorption near edge structure (XANES) spectra. The best fit was found to be the four nearest N coordination shell followed by two carbon shells (Figure 5E). The as-synthesized NiSA-N-CNTs electrocatalysts delivered an impressive catalytic activity toward the electrochemical reduction of CO_2 to CO with ultrahigh Faradaic efficiency (FE) values of 89.0% and 91.3% at −0.55 and −0.7 V (Figure 5F). The rational design of Ni-SACs onto 1D nanocarbon networks have undoubtedly emerged as a powerful strategy to build ultraefficient CO_2-to-CO electrocatalysts.

2D nanomaterials show particularly unique features compared with other dimensional structures.[100] For example, the metal single atoms supported on 2D materials tend to be more coordinatively unsaturated and are more easily to be exposed to catalytic species, which guarantees high metal loadings and enlarges the electrocatalytic activities compared with their 0D and 1D counterparts. Among the 2D nanostructures, graphdiyne (GD) constitutes a rising star electrocatalytic nanomaterial, which is composed by a one-atom-thick 2D architecture with natural uniform pores and triple bond rich with strong reduction ability.[101,102] GD can also be used as a nanocarbon platform without any pretreatment, providing a unique opportunity to fabricate stable atomic catalysts. In this direction, a scalable, efficient, and universal electrochemical synthetic strategy has been developed to build Fe/GD and Ni/GD SACs.[86] The Fe/GD and Ni/GD SACs were prepared through a two-step synthetic methodology. The first step consisted in the preparation of 3D GD foam (GDF) on carbon cloth surfaces using an acetylenic cross-coupling reaction and hexaethynylbenzene (HEB) as precursor. Second, the Ni/Fe atoms were anchored onto the GD surfaces by a facile electrochemical reduction method (Figure 5G). To confirm that the as-synthesized Fe/GD and Ni/GD SACs are formed by atomically dispersed Ni/Fe atoms, XANES and extended X-ray absorption fine structure (EXAFS) experiments were performed. Remarkably, the Ni/GD exhibited only one notable peak at ≈1.6 Å from the Ni—C contribution and no peak in the region 2–3 Å from the Ni—Ni contribution, revealing that Ni appears mainly as isolated atoms in the GD network (Figure 5H). Additionally, the Fe/GD and Ni/GD SACs displayed Pt-like HER electrocatalytic properties (Figure 5I) due to the acute interfacial interactions and electronic coupling between the Ni/Fe atomic centers and the GD, which allow high degrees of charge transport from the 2D-platform to the catalytically active metallic sites. This work launched a universal, low-cost, and scalable synthetic strategy towards the construction of atomically dispersed TMs onto 2D nanocarbons as excellent atomic electrocatalysts.

5.2. ACEs onto 0D, 1D, and 2D Platforms: Structural Properties

ACEs represent a new class of nanomaterials that are currently emerging as rising start catalysts in the field of electrocatalysis due to their fascinating structural properties such as high surface-to-volume ratio, well-defined chemical compositions, and atomic structures as well as a plenty of tunable active sites for catalytic reactions that usually take place at electrochemical interfaces, which maximize the atom utilization and boost the overall electrocatalytic rates.[105]

With the giant breakthroughs in the development of advanced characterization methods, the structure, active sites, and catalytic mechanisms of ACEs have been progressively unlocked. For example, HAADF-STEM, EXAFS spectra, and XANES spectra can all be used to entirely understand the physical and chemical features of the as-synthesized electrocatalysts.[106,107] Furthermore, density functional theory (DFT) calculations have been very useful to study the electrocatalytic active sites, thus enhancing our knowledge about the electrocatalytic pathways on the surfaces of ACEs.[1,108,109]

Most importantly, the structural control of the metallic clusters of ACEs is becoming a new strategy to finely tune the reactivity and, in turn, the intrinsic catalytic properties of their catalytically active centers, thus promoting the activation of ultractive hot spots for different electrocatalytic processes.[8,79] Nanocarbon platforms with different dimensionalities have been used to support different types of atomic clusters, thus regulating a bunch of ion migration processes together with the energetic levels of adsorbed intermediate catalytic species in key catalytic reactions like oxygen reduction reaction (ORR), oxygen evolution reaction (OER), nitrogen reduction reaction (NRR) and CO_2 electroreduction reaction (CO_2RR).[96] The metal–nanocarbon interfacial interaction between the anchored metal atoms and the LD carbon networks also plays a paramount role in many electrocatalytic processes.[110] Additionally, the electron transfer (ET) among nanocarbon supports and metal species represents a significant phenomenon that usually has led to the variation of charge states of the subnanometer metallic clusters, thus influencing the charge density and distribution of metal species, which regulate the electrocatalytic pathways of the overall catalytic reactions.[111–113] Remarkably, ET processes between tiny metallic clusters and nanocarbon platforms could be controlled by the size of metal particles and the geometry of the metal species in the clusters, thus opening a new avenue towards the rational design of low-nuclearity electrocatalytic systems that exhibit superior advantages for multifunctional electrocatalysis.[114,115]

The development of low-nuclearity electrocatalysts with 0D-nanocarbon platforms is scarcely seen in the literature. Only a few examples of 0D nanocarbon architectures have been employed as LD platforms to fabricate ACEs. Markedly, entrapping small metallic cluster onto carbon nanocages to form endohedral fullerenes (EMFs) have become a suitable synthetic strategy to fabricate atomic cluster 0D-nanomaterials.[116,117] They contain additional atoms, ions, or clusters enclosed within their inner carbon spheres and exhibit promising electronic properties for a myriad of electrocatalytic reactions as a result of the electronic wiring between the inner metallic clusters and the carbon nanocages. Nonetheless, the disentangling of the electrocatalytic properties of these peculiar 0D-metallocluster nanomaterials have been widely elusive up to now. In a pioneering work, Santiago and colleagues disclose for the first time the underlying factors that govern the HER

electrocatalytic behavior of seven $M_3N@C_{2n}$ ($2n$ = 68, 78, and 80) fullerenes using an elegant combination of experimental and theoretical techniques.[103] The role of the metal, symmetry, number of carbon atoms, and non-IPR sites towards the efficient production of molecular hydrogen of $Gd_3N@I_h(7)$-C_{80}, $Y_3N@I_h(7)$-C_{80}, $Lu_3N@I_h(7)$-C_{80}, $Sc_3N@I_h(7)$-C_{80}, $Sc_3N@D_{5h}(6)$-C_{80}, $Sc_3N@D_{3h}(5)$-C_{78}, and $Sc_3N@D_3(6140)$-C_{68} EFMs were thoroughly explored (**Figure 6**A). Remarkably, they concluded that the structural variations among the metallic clusters such as the nature of the metal, symmetries, and degree of pyramidalization do not fulfill a substantial role in their HER catalytic activities. Most importantly, the non-IPR $Sc_3N@D_3(6140)$-C_{68}, which exhibit three negatively charged pentalene units that stabilize the electronic structure of the nanocages, delivered by far the

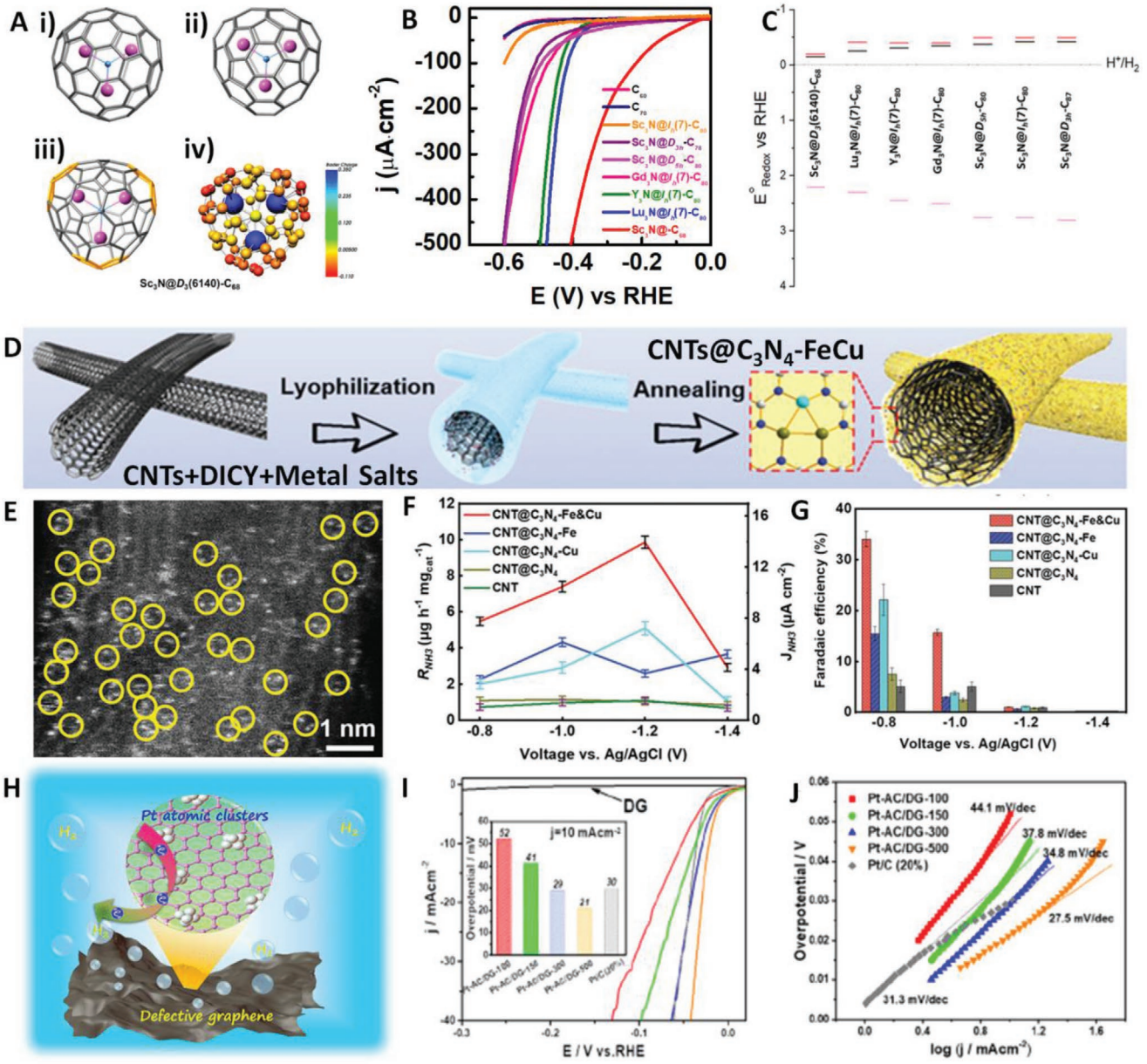

Figure 6. A) Ball-and-stick representation for i) $Sc_3N@I_h(7)$-C_{80}, ii) $Sc_3N@D_{3h}(5)$-C_{78}, and iii) $Sc_3N@D_3(6140)$-C_{68} HER electrocatalysts as well as the iv) computed atomic charges for $Sc_3N@D_3(6140)$-C_{68}. B) HER polarization curves for C_{60}, C_{70}, $Gd_3N@I_h(7)$-C_{80}, $Y_3N@I_h(7)$-C_{80}, $Lu_3N@I_h(7)$-C_{80}, $Sc_3N@I_h(7)$-C_{80}, $Sc_3N@D_{5h}(6)$-C_{80}, $Sc_3N@D_{3h}(5)$-C_{78}, and $Sc_3N@D_3(6140)$-C_{68} and Pt/C at 2 mV s^{-1} in 0.5 M H_2SO_4. C) Mott–Schottky (M–S) analyses for the EMF electrocatalysts. Adapted with permission.[103] Copyright 2020, American Chemical Society. D) Schematic diagram of the synthetic strategy for CNT@C_3N_4—Fe&Cu NRR catalysts. E) HR-STEM image of CNT@C_3N_4—Fe&Cu catalysts. F) NH_3 yield rate and partial current densities of the as-synthesized subnanometer clusters at different potentials and their corresponding G) FEs. Adapted with permission.[105] Copyright 2021, American Chemical Society. H) Schematic illustration of the carbon-defect-driven electroless deposition of Pt-ACs onto DG. I) LSV curves of the HER (inset with the η_{10} values) on Pt-AC/DG-X and benchmark Pt/C (20%) catalysts at a scan rate of 5 mV s^{-1} and their corresponding J) Tafel plots. Adapted with permission.[79] Copyright 2020, American Chemical Society.

best HER performance among all the EMFs showing a very low onset potential of −38 mV versus RHE and an enhanced current density of 500 μA cm^{-2} at −0.4 V versus RHE (Figure 6B). Definitely, it was demonstrated that the different structural organization of the carbon atoms in the cage of the $Sc_3N@D_3(6140)$-C_{68} compound plays a paramount role in the HER mechanism. The unique electronic properties of the pentalene units (high local electronic density) can significantly reduce the LUMO energy values toward the proton adsorption, thus promoting the hydrogen protonation into the nanocage surface and, in turn, boosting the overall electrocatalytic rates. The Mott–Schottky analyses of the EMFs strongly confirmed that the calculated Fermi level for $Sc_3N@D_3(6140)$-C_{68} is the closest value to that for the standard hydrogen evolution potential (0 eV), which widely facilitates the reduction of the hydrogen atoms after the protonation step (Figure 6C). This work shed light on the electrocatalytic pathways of low-nuclearity electrocatalysts formed by 0D nanocarbon surfaces and metallic atomic clusters.

The utilization of 1D-nanocarbon networks with unique microenvironments to precisely confine small metallic clusters is emerging as a desirable strategy to build ACEs.[118–120] Such confinement not only provides strong interactions between the reactants and the catalytic active species at 1D surfaces, but also leads to potential synergetic effects, enhancing the intimate contact between multiple active species and favoring the efficiency of many catalytic reactions, especially multistep catalytic processes such as NRR and CO_2RR. As an ideal 1D platform, multiwall CNTs (MWCNTs) exhibit excellent electric conductivities, huge specific surface areas, and a lot of potential anchoring points as supports for tiny metallic clusters. The CNTs can effectively anchor Pt atoms by avoiding migration and aggregation deriving from high surface energy environments. Xiawei Wang and colleagues extended the concept of nanoreactors to subnanoreactors in 1D-surfaces by confining clusters of Fe and Cu atoms in the surfaces of carbon nitride decorated MWCNTs (CNT@C_3N_4—Fe&Cu) for superior NRR electrocatalysis.[104] To synthesize the Fe-Cu ACEs MWCNTs were used were softly oxidized to obtain a better affinity with dicyandiamide (DICY) precursor and metal salts ($FeCl_2$ and $CuCl_2$ with a molar ratio of 1:1) in an aqueous solution. The obtained composite was subsequently annealed in an inert atmosphere to generate the CNT@C_3N_4—Fe&Cu electrocatalytic heterostructure (Figure 6D). Notably, the as-synthesized Fe—Cu atomic clusters were uniformly distributed into the 1D-carbon nanostructure CNT@C_3N_4 network as shown by STEM images at high-resolution. (Figure 6E). Remarkably, the coordination between Cu and Fe in subnanometer clusters parallelly accelerate the adsorption of N_2, thus optimizing the reaction pathway toward a lower energetic barrier and leading to impressively better NRR catalytic rates than those of their monometallic counterparts (Figure 6F,G). This seminal work paves the way towards the design of a new generation of 1D-ACEs with a highly accurate spatial distribution of the atomic clusters for a large portfolio of catalytic reactions.

2D graphene-based nanomaterials have been widely used as suitable platforms to anchor atomic clusters for electrocatalytic purposes because of their unique structure of 2D sheet composed of sp^2-bonded carbon atoms with one-atomic thickness as well as their superior electric conductivities and remarkable mechanical and electrical properties.[121–123] Liming Dai and colleagues have developed an innovative strategy to fabricate very small, well-defined, and ultrastable atomic Pt clusters anchored onto DG nanoplatforms (Pt-AC/DG) using a one-step carbon-defect driven electroless deposition method (Figure 6H).[79] The carbon defects of the 2D-graphene networks exhibit a lower work function and higher reducing capacity compared to those of the defect-free graphene structures, thus facilitating the preferential adsorption and reduction of Pt ions at the defective sites of the nanocarbon networks and promoting the formation of ultrastable atomic Pt clusters with accessible catalytic centers. Therefore, the as-synthesized Pt-AC/DG ACEs delivered a superb electrocatalytic activity toward the generation of molecular hydrogen (HER), surpassing the efficiency and stability of benchmarks Pt/C catalysts (Figure 6I,J), opening new pathways to produce low cost-Pt based catalysts with extraordinary electrocatalytic properties.

6. Electrocatalytic Applications of SACs and ACEs Supported on LD Nanomaterials

6.1. Electrocatalytic Applications of SACs and ACEs for ORR, HER, and OER

Renewable energy storage and conversion technologies such as fuel cells, metal–air batteries, and water splitting systems are promising alternatives to traditional fossil fuels.[127–130] The electrochemical ORR, OER, and hydrogen evolution reaction (HER) are at the heart of several clean energy technologies.[6,110,131,132] Remarkably, reducing the size of the metal particles to nanoclusters or single atoms to construct both SACs and ACEs has drawn a lot of attention as a successful strategy to decisively improve the electrocatalytic rates of the above-mentioned electrochemical reactions.[133,134] Among the factors that promote the enhanced electrocatalytic performances of low-nuclearity electrocatalysts can be found: i) low-coordination environment of active single or cluster catalytic centers; ii) size effect, where confinement of electrons leads to discrete energy level distributions; and iii) strong metal–nanoplatform interfacial interactions, which will facilitate an intimate electronic communication between them, thus decreasing the energetic states of intermediates reagents and promoting outstandingly good electrocatalytic performances.[135,136]

Importantly, it is worth noting that compared with SACs, ACEs exhibit larger metal loadings and more sophisticated and flexible active sites towards ORR, HER, and OER reactions, thus attaining superior catalytic performances and providing better opportunities to develop highly efficient multifunctional electrocatalytic systems. ACEs offer new chances towards the successful regulation of the electronic and catalytic properties of low-nuclearity architectures. Besides, it has been theoretically demonstrated that small noble metal clusters can potentially break the scaling relations due to their extraordinary fluxional behavior and the poor correlation between binding energies of the intermediates such as O*, OH*, and OOH*, which could open new opportunities to fabricate more active water splitting electrocatalysts.[137]

The understanding of the structure-catalytic function relationships of SACs has been thoroughly investigated in the recent years.[1,109,138] Nonetheless, there is a lack of knowledge about the proximity effects of neighboring single metal atoms for ORR, HER, and OER reactions, which have been limited the design of more powerful atomic electrocatalysts due to the lack of details on the intrinsic activity of individual atomic sites and the mass transport of intermediate species. Fortunately, Guihao Yu and coworkers have elegantly reported a comprehensibly microscopic, electrochemical, spectroscopic, and theoretical study about the connection between the atomic distribution density of Fe-N_4 SACs and their resulting ORR electrocatalytic rates.[124] Initially, they prepared a bunch of atomically distributed Fe centers with controllable density on nitrogen-doped carbon networks using a hydrogel-anchoring strategy. The clear peak assigned to the Fe—N bond and the no appearance of Fe—Fe interactions in the EXAFS spectra of Fe-SACs with different inter-site atomic distances revealed that the Fe sites of the as-synthesized atomic electrocatalysts are uniformly distributed into the nanocarbon network (**Figure 7**A,C). The atomic distribution of the Fe centers allowed an accurate analysis of the correlation among the d_{site} and the ORR electrocatalytic activity of Fe-SACs. Strikingly, it was discovered that the electronic among adjacent Fe sites can greatly boost the overall ORR electrocatalytic activity of SACs (Figure 7B), demonstrating that the SACs with lower Fe loadings are the much more successful ORR catalysts. Furthermore, they calculated the TOF number as function of d_{site} to gain a quantitative knowledge of how the inter-site distance can control the intrinsic catalytic activity of Fe-SACs. Notable differences were observed in samples with lower Fe loadings, in which the TOF number experimented an almost linear trend with the increment of d_{site} (Figure 7D). This seminal work has unlocked crucial insights into the kinetic behavior of atomically dispersed Fe centers as a function of the inter-site distance (d_{site}), thus promoting the upcoming fabrication

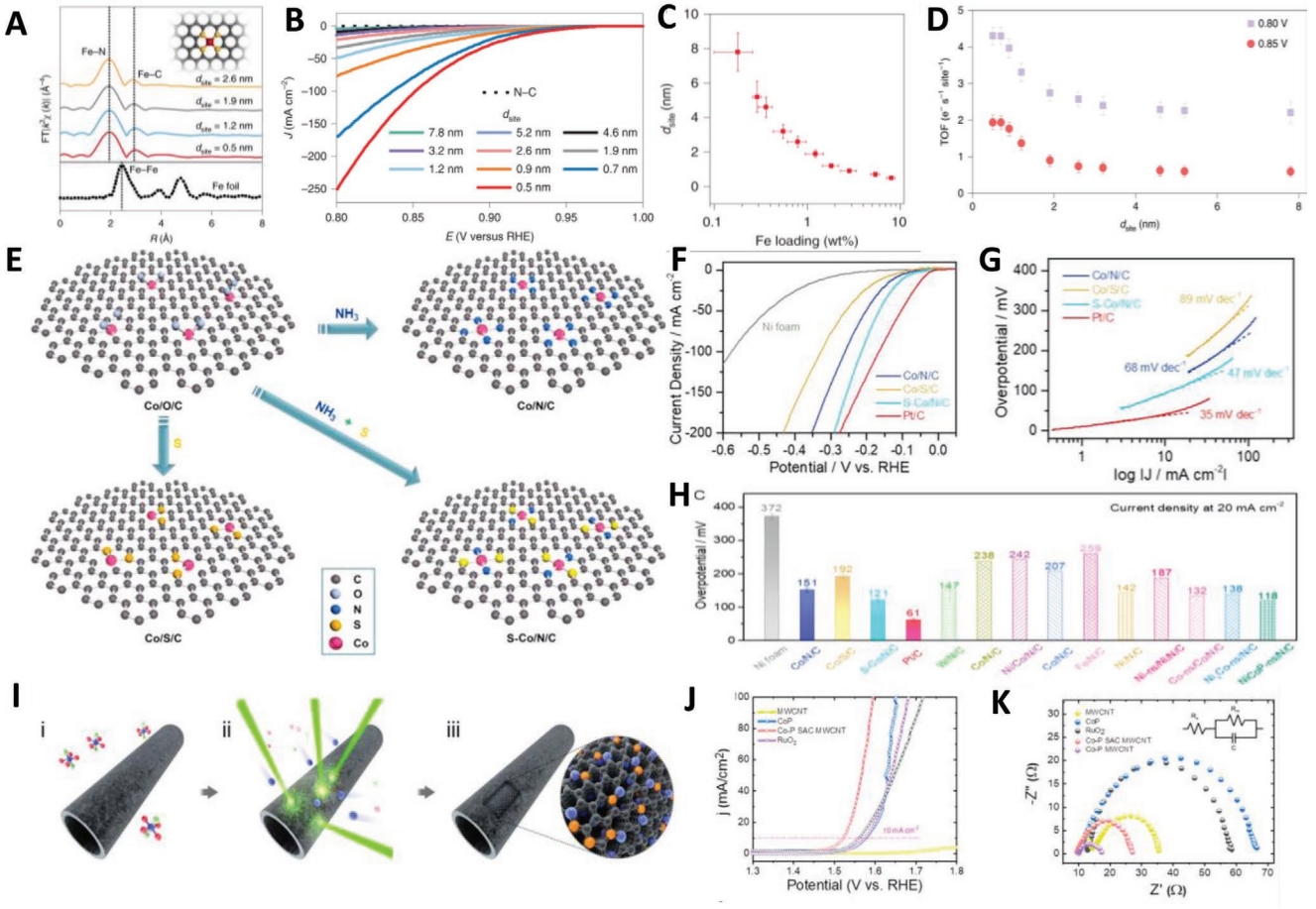

Figure 7. A) Fourier-transform magnitude function of phase-corrected EXAFS spectra for four typical Fe—N_4 SACs with d_{site} = 0.5, 1.2, 1.9, and 2.6 nm and Fe foil as the reference. B) ORR polarization curves of the Fe—N_4 SACs with different d_{site} values. C) Correlation of Fe contents and site densities with different d_{site} values. D) TOF numbers as a function of d_{site}. Adapted with permission.[124] Copyright 2021, Nature Publishing Group. E) Illustration of the synthesis of Co-SACs with different coordination environments using graphene as carbon nanoplatform. F) LSVs of the HER processes for Co-SACs in KOH solution and their corresponding G) Tafel plots. H) Comparison of the Co-SAC electrocatalytic performances with the state-of-the-art HER catalysts. Adapted with permission[125] Copyright 2021, American Chemical Society. I) Schematic illustration of material design concept for Co—P SAC MWCNT using PLC process in liquid. J) OER polarization curves (scan rate 5 mV s^{-1}) for Co-SAC MWCNT (blue), P-SAC MWCNT (gray), and Co—P SAC MWCNT (red) catalysts in an O_2-saturated 1.0 M KOH solution and their corresponding K) Nyquist plots. Adapted with permission.[126] Copyright 2021, American Chemical Society.

of highly dense SACs for a large portfolio of electrocatalytic reactions.

The effect of the local coordination environment of atomic catalysts has been recently explored.[139] Tao Sun and colleagues elegantly discovered the influence of the first coordination sphere of Co-SACs in the electrochemical generation of molecular hydrogen.[125] They synthesized Co-SACs with different coordination environments (S-Co/N/C, Co/N/C, and Co/S/C) in graphene networks using a simple pyrolisis strategy (Figure 7E). The HER polarization curves and the corresponding Tafel plots showed significant variations in the electrocatalytic behavior of the Co-SACs electrocatalysts, verifying that S doping into Co/N/C leads to higher HER electrokinetics (Figure 7F,G). Remarkably, the HER performances of the as-synthesized Co-SACs are well-ranked among the state-of-the-art non-precious HER catalysts reported up to date (Figure 7H). These results shed light on the effects of the first coordination environments of Co-SACs on their electrocatalytic activities.

Using an ultrafast pulsed laser confinement (PLC) process, atomic cobalt (Co) and phosphorus (P) high loading densities were uniformly anchored on the outer walls of 1D-MWCNT to fabricate robust heteroatom-doped Co-SACs electrocatalysts for OER (Figure 7I).[126] Impressively, the overpotential for delivering a current density of 10 mA cm^{-2} (η_{10}) of Co-P SAC MWCNT (290 mV) surpassed by far the value obtained for the benchmark RuO_2 catalyst (390 mV), which was attributed to the close electronic interactions between catalytic Co atomic sites and highly conductive MWCNTs (Figure 7J,K). This work launched a practical SAC design strategy that could benefit the future commercialization of these nanocatalysts.

The confinement of small size atomic clusters onto LD nanocarbons is emerging as a suitable strategy to fabricate ultraactive ORR, HER, and ORR electrocatalysts. Engineering the geometry of subnanometer metallic clusters offers a plenty of possibilities to design more productive active sites towards water-involved electrochemical reactions due to each specific cluster geometry gives rise to a particular interfacial electronic distribution, which, in turn, significantly changes the adsorption energy states of many reactants and intermediate catalytic species and their overall electrocatalytic efficiencies.

Lichen Bai and coworkers have smartly achieved the formation of non-precious dual atom OER electrocatalysts via in situ electrocatalytic transformation of purposely designed Fe, Ni, Co-SACs.[140] They found that the Fe, Ni, and Co-SACs were nicely converted to Co—Fe, Fe—Ni, and Co—Fe double-atom catalysts by adding a second metal ion from the electrolyte into the nanocarbon network under OER experimental conditions. The initial SACs rendered very poor OER performances as seen in the linear scan voltammetry curves of the monometallic electrocatalysts (**Figure 8**A). Nonetheless, the OER activities were drastically improved upon constant current electrolysis at 2 mA cm^{-2} in a commercial KOH solution that contained low amounts of a second metal (Figure 8A,B), thus indicating the construction of dual-atom nanostructures. Most importantly, both the thermodynamic (η_{10}) and kinetic (Tafel slope) electrochemical parameters of the single atom precursors were notably boosted after their in situ electrochemical transformations to double atom electrocatalysts (Figure 8A,B), suggesting that the catalytic improvement was triggered by the synergistic cooperation amongst the two atomic metal species, which decisively benefit the energy states of key OER intermediate species. Additionally, the double atom cluster electrocatalysts displayed largely bigger intrinsic catalytic activities as shown in Figure 8C. The as-synthesized double atom cluster electrocatalysts represent an attractive platform to get an in-depth understanding of the mechanistic pathways of heterogeneous OER ACEs. In another excellent example of ACEs, Lou and colleagues have stated that Pt-based clusters in nanostructured carbon hosts can remarkably catalyze the generation of molecular hydrogen.[105] The resulting heterostructure ACE (denoted as Pt_5/HMCS) exhibited a very high density of precious Pt atoms into the nanocarbon structure. Noticeably, the entrapped Pt clusters delivered an enhanced stability and ultralow tendency of agglomeration as well as excellent HER electrocatalytic properties. The low HER activity of Pt-free HMCS as the blank control verifies that the superior electrocatalytic activity of the Pt_5/HMCS ACE, in both acid and basic environments, is arisen from the Pt clusters (Figure 8D,E). Additionally, in both acidic and alkaline conditions, the HER LSVs display a small shift of around 3 mV at $j = 10$ mA cm^{-2} after 3000 cycles (Figure 8F), thus exceeding by far the durability properties of Pt benchmark catalysts. ACEs have been also designed to act as ultraefficient ORR electrocatalysts. A cost-effective and scalable in situ nitriding approach have been used to fabricate tungsten nitride atomic clusters anchored on 2D g-C_3N_4 nanosheets (WN@g-C_3N_4) using NaCl-template and urea as precursors.[141] The homogeneously distributed cubic phase WN atomic clusters behave as ultractive active sites for the ORR in alkaline solution, which is comparable to benchmark Pt/C catalyst, most likely because of the large surface area and the excellent intrinsic catalytic activity. (Figure 8G–I) The stable 2D g-C_3N_4 nanocarbon platform together with the large number of the W—N bonds promotes better flexibility and electronic transfer to the entire nanoheterostructure, leading to an efficient 4-electron ORR pathway (Figure 8I). This work revealed the paramount importance of WN atomic clusters for superior ORR electrocatalysis.

6.2. Electrocatalytic Applications of SACs and ACEs for NRR and CO_2RR

Converting CO_2 and N_2 into high added-valuable chemicals or fuels using green electricity under soft conditions has gained an enormous interest for both environmental protection and market economies.[142–145] Due to the relatively stable nature of CO_2 and N_2, high overpotentials are usually applied to surpass the activation barriers and generate reasonable currents. Importantly, once certain overpotential is applied, the HER can easily become a significant competitor in a large portfolio of catalytic materials. Thus, a suitable selective CO_2 or N_2 electrocatalyst should exhibit not only excellent electronic properties to promote the multistep catalytic pathways of the aforementioned reactions but have to notably suppress the competitive HER.

Non-precious TMs such as Fe, Co, and Ni, which usually exhibit decent HER activities, have been scarcely chosen as compelling electrocatalytic candidates for CO_2-to-CO conversion or NRR. Nonetheless, their electronic structures can be finely tuned once dispersed into single atoms or small atomic

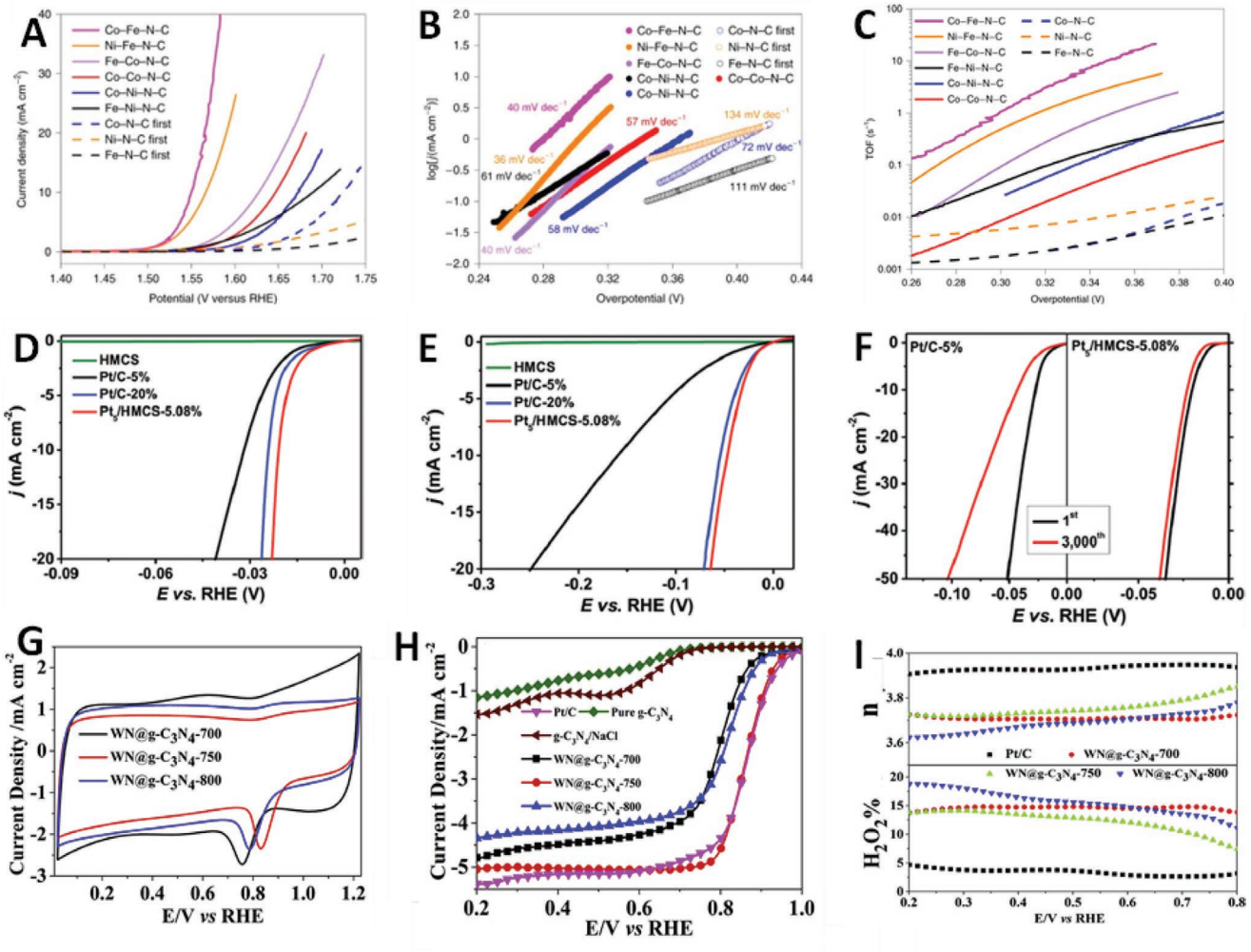

Figure 8. A) OER polarization curves of single-atom precatalysts (dashed lines) and double-atom catalysts (solid lines) in 1 M KOH and their corresponding B) Tafel plots. C) TOF numbers of single and dual atomic catalysts as a function of potential. Adapted with permission.[140] Copyright 2021, Nature Publishing Group. Electrocatalytic hydrogen evolution using Pt5/HMCS electrocatalyst and its comparison with Pt/C benchmark in D) 0.5 m H_2SO_4 and E) 1.0 m KOH. F) Polarization curves of Pt/C-5% (left) and Pt5/HMCS-5.08% (right) after continuous potential sweeps at 50 mV s^{-1} in H_2SO_4. Adapted with permission.[105] Copyright 2020, Wiley. G) CV curves of WN samples at a scan rate of 50 mV s^{-1} in 0.1 M KOH solution. H) ORR LSV curves of as-synthesized tungsten nitride ACEs including Pt/C recorded in 0.1 M KOH and 0.1 M $HClO_4$ solution at a rate of 10 mV s^{-1}. I) Electron number transferred per oxygen molecule and $\%H_2O_2$ generation for the tungsten nitride ACEs.

clusters, leading to many advantageous structural and electronic properties towards NRR and CO_2RR. SACs and ACEs exhibit remarkable long-term electrochemical stability properties due to the strong chemical bonding between the single and/or atomic clusters and LD nanocarbon substrates. Besides, because of the electronic confinement, discrete energy levels are formed around the Fermi level, which benefits the surface interaction of the active centers with reactants and intermediates. Finally, the unsaturated local coordination environment of SACs and ACEs offers a lot of opportunities to design new NRR and CO_2RR active sites with fascinating electrocatalytic properties.[146–149]

Kun Jiang and coworkers have reported a new class of Ni SACs using 2D-graphene as nanocarbon platform for highly active and selective CO_2 to CO electroreduction.[150] CO_2-to-CO electroreduction process begins from –0.31 V versus RHE and quickly increases to an 83% of the CO FE at an overpotential of 480 mV, keeping a plateau of more than 90% CO FE until –0.87 V (**Figure 9**A,B). Charge density distribution DFT calculations led to a deeper understanding of the excellent catalytic activity of Ni-SACs (Figure 9C). The C or N atoms located in the surroundings of the atomically dispersed Ni centers can reduce the electronic density of the metallic SAs, thus lowering the desorption barriers for key catalytic intermediates such as CO* and COOH*. This seminal study established that TM SAs onto 2D platforms can be used as promising CO_2RR electrocatalysts by tailoring the electronic clouds of the metallic centers. Non-precious Cu-SACs based on porous nitrogen-doped carbon network (NC-Cu SA) were built for high-performance NRR electrocatalysis.[151] The NC-Cu SA delivered remarkable FEs of 13.8% and 11.7% and huge NH_3 yield rates of ≈53.3 and ≈49.3 μg_{NH3} h^{-1} mg_{cat}^{-1} in 0.1 M KOH and 0.1 M HCl electrolytes, respectively (Figure 9D–F). The well-dispersed of Cu-SAs attached into porous N-doped carbon triggered the nucleation

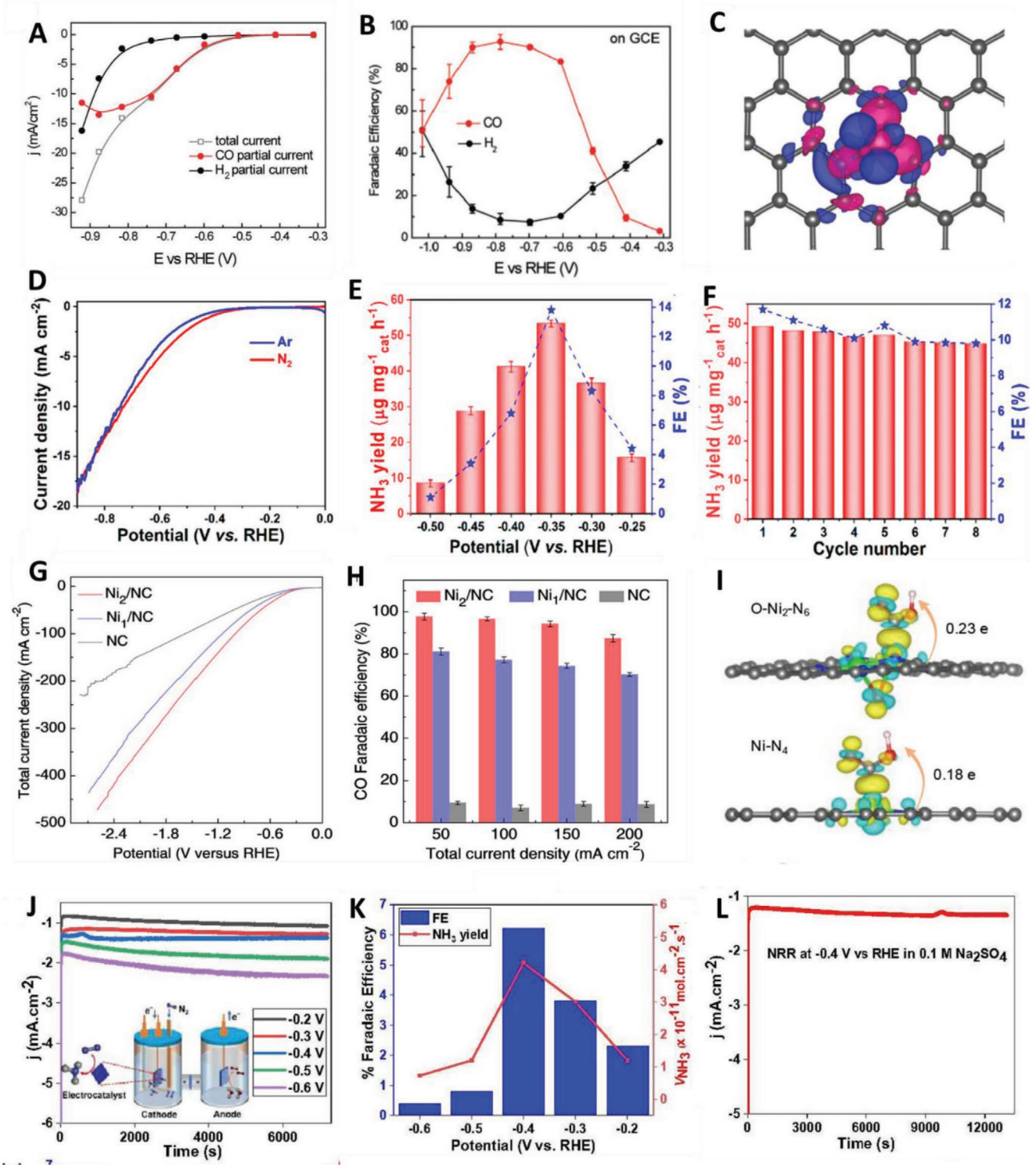

Figure 9. A) Steady-state current densities and the B) corresponding FEs of H_2 and CO on a GCE in CO_2-saturated 0.5 M $KHCO_3$ for Ni-NG. C) Charge density distribution of the Ni single atoms confined in graphene vacancies. Adapted with permission.[150] Copyright 2018, Royal Chemistry Society. D) LSV curves in N_2-saturated and Ar-saturated 0.1 M KOH electrolytes, E) NH_3 yield rate and FE at different potentials in 0.1 M KOH, and F) NH_3 yield rates with increasing cycle numbers in 0.1 M HCl for NC-Cu SA. Adapted with permission.[151] Copyright 2019, American Chemical Society. G) LSV curves in the CO_2-flowed 1.0 M $KHCO_3$ electrolytes their corresponding H) CO FE values for Ni_2/NC, Ni_1/NC, and NC catalysts. I) Electron density difference plot of the *COOH intermediate adsorption structure on O—Ni_2—N_6 and Ni—N_4 and the Bader charge analysis. Adapted with permission.[152] Copyright 2021, American Chemical Society. J) CA curves of $CoFe_2O_4$/rGO in 0.1 Na_2SO_4. Inset: electrochemical cell. K) FE and NH_3 yield values for the $CoFe_2O_4$/rGO ACEs. L) Electrochemical stability of the ACEs. Adapted with permission.[153] Copyright 2019, Royal Chemistry Society.

of highly active Cu-N_2 sites, which give rise to more energetically favorable NRR distal pathways, boosting the overall NRR rates.

The development of ACEs for NRR and CO_2RR electrochemical reactions has become a hotspot in the field of electrocatalysis. Particularly, atomically precise subnanometer metal clusters (organic ligand-stabilized metal centers) represent a unique type of atomic materials which exhibits ideal molecular purity, well-defined composition, and desirable structural properties for the above-mentioned electrocatalytic reactions. In this regard, Tao Ding and coworkers have successfully prepared highly uniformly distributed dinuclear Ni sites into nitrogen-doped carbon substrates (Ni_2/NC) using ligand-coordinated dual atom precursors ($Ni_2(dppm)_2Cl_3$).[152] The Ni_2/NC ACE displayed a lower onset potential towards the electrochemical reduction of CO_2, which is much better than that of the SA counterpart (Ni_1/NC) at the scan rate of 5 mV s^{-1} (Figure 9G). Furthermore, the Ni_2/NC ACE delivered a CO FE of 94.3% at the current density of 150 mA cm^{-2}, which is at least 1.3 times higher than the FE value obtained for Ni_1/NC (Figure 9H). It was determined that the coordinated unsaturated diatomic Ni centers can promote a facile adsorption of oxygen species and form an optimized O—Ni_2—N_6 structural configuration that is capable of substantially decreasing the energy barrier for the activation of CO_2 to COOH* (Figure 9I). Chuan Zhao and colleagues developed a new type of ACEs based on $CoFe_2O_4$ nanoclusters/graphene nanoheterostructures for NRR.[153] The as-synthesized catalyst delivered very competitive FE and NH_3 yield rate values which are comparable with those of the top-ranked NRR catalysts published up to now (Figure 9J,K). Furthermore, the $CoFe_2O_4$ nanoclusters/graphene ACE showed excellent long-term electrochemical properties for NRR at –0.4 V versus RHE. These findings opened the doors towards the simple fabrication of bimetallic nanoclusters on graphene or other 2D supports for NRR at ambient conditions.

7. Theoretical Advances in the Mechanistic Pathways

Theoretical calculation and simulation techniques provide a powerful tool to deeply reveal the origin of the catalytic mechanism of atomic catalysts by efficiently screening out the most promising candidates.[154] As we know, the essence of a catalytic reaction is the breaking of old bonds and the formation of new bonds that all occur at the atomic level. DFT methods have matured to the level and have shown an increasingly significant role in understanding the reaction mechanism at atomic level nowadays. The catalytic performances including activity, selectivity, and stability of single atom and subnanometer atomic clusters electrocatalysts could be affected by many factors, such as the size, different coordination environments, complex interactions with supports, confinement catalytic systems, applied strain, and so on. All of these influences can be worked separately or together to finally decide the catalytic performance. In this section, we focus on the theoretical perspective to elaborate the above-mentioned factors in tuning the catalytic performance and provide useful strategies to rational design highly efficient single atom and subnanometer atomic clusters electrocatalysts.

7.1. Size and Morphology Effect

The in-depth understanding of "structure-performance" relationship plays a vital role in developing new robust electrocatalysts. Subnanometer atomic catalysts including single,[158–160] dimer,[161–163] triple, and small atomic clusters generally exhibit different catalytic behaviors because of various sizes and structures of the active sites. The precise control of the size of cluster can tune the catalytic performance. Theoretical researchers take advantages of the state-of-the-art quantum chemical methodologies to build models to simulate the catalytic process. On one hand, different size of atomic clusters loading on the same LD nanostructures could demonstrate different catalytic mechanism.[164] He et al. systemically investigated the electrochemical reduction of carbon dioxide on precise number of Fe atoms anchored graphdiyne (GDY) (**Figure 10**A) by using DFT calculations.[155] They found that the catalytic activity and selectivity had dependent on the number of Fe atoms. The smaller Fe clusters favor the multi-electron (>2e$^-$) reactions and small Fe clusters tend to two-electron reaction. For instance, Fe@GDY and Fe_2@GDY can efficiently converse CO_2 into CH_4 products, while Fe_3@GDY and Fe_4@GDY preferred to generate HCOOH. The reason mainly attributes to the different affinity of *CO, *CHO, and *OCHO that can be changed on different number of Fe atoms which results in catalytic efficiency and product selectivity for CO_2RR. They also pointed out that the reactivity of Fe pair active site outperforms the single Fe atom, which further indicated the strategy of controlling the size of active sites to boost the catalytic performance. Moreover, heterogenous dimer atomic clusters have been emerging as a new class of electrocatalysts with improved catalytic performance.[109] The asymmetry active sites can work synergistically in the reaction and the activity and selectivity can be tuned by selecting appropriate combinations.[161–163] The electronic properties of subnanometer atomic clusters can also be modified by tuning the size of the atoms. When loading the metal clusters onto the LD materials, the oxidation of the metal atoms has significant influence on the binding strength of the intermediates during the reactions. For CO_2 reduction to C_{2+} products, the most challenging step is the C—C coupling which needs ultra-high energy input. Ling et al. theoretically designed a Cu_4 cluster supported on g-C_3N_4 nanosheet catalysts to capture and reduce CO_2 into C_2H_5OH.[156] The Cu atoms connected to g-C_3N_4 can be oxidized to Cu^{x+} because of the charge transfer from the Cu atoms to the substrate, while the upper Cu atom maintained the Cu^0 oxidation (Figure 10B). The mixed Cu^0 and Cu^{x+} state in the active sites can greatly decrease the energy barrier of the C—C coupling, leading to the formation of the final C_2 product. Moreover, the different size of atomic clusters shows different structure, energetic, and magnetic properties on the LD materials.[165] Silva et al. compared the adsorption behavior of small Ni_n, Pd_n, and Pt_n clusters (n = 1 to 6) on the graphene monolayer.[166] They found that the interaction between the clusters and the support becomes weak with the increase of the n number. The adsorption leads to the charge redistribution between the metal clusters and graphene. The Ni clusters transfer three times large electrons to the graphene than Pt and Pd clusters. These different binding structures and oxidation of the metals

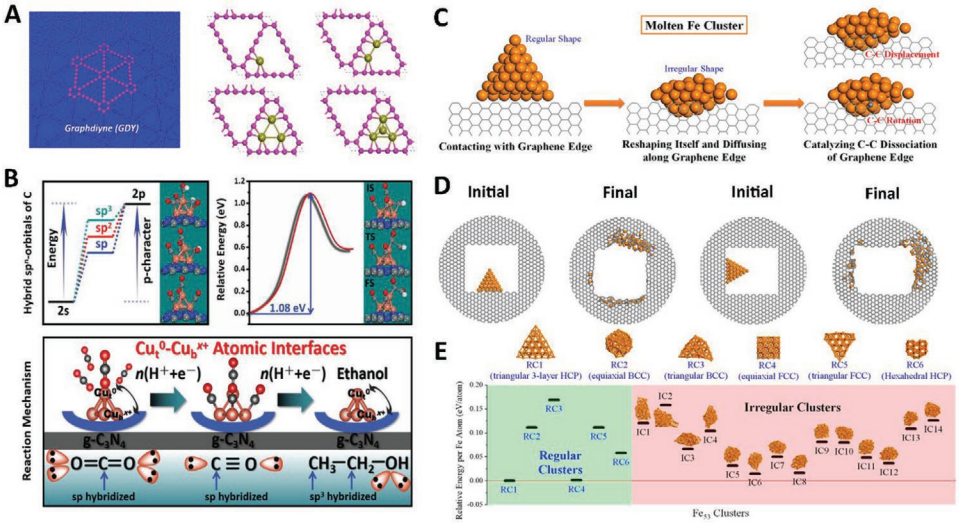

Figure 10. A) Schematic illustration of the single Fe atom, Fe dimer, Fe triple, and Fe_4 cluster anchored on 2D graphdiyne (GDY) nanosheet. Adapted with permission.[155] Copyright 2020, Elsevier. B) Schematic molecular orbital energy diagram, energy barriers for C—C coupling, and reaction mechanism for CO_2 reduction into ethanol on Td-Cu_4@g-C_3N_4. Adapted with permission.[156] Copyright 2018, Wiley. C) Sketch of structure evolution from regular shape to irregular shape of Fe_{53} cluster on graphene. D) The initial and final states of Fe_{53} cluster on graphene after 100 ps reactive MD simulations. E) Comparison of relative energies of various Fe clusters with 53 atoms. Adapted with permission.[157] Copyright 2019, American Chemical Society.

clusters could alter the reaction pathways and govern the final products.

Besides the size of the subnanometer atomic clusters, the morphology of the cluster also plays an important role in catalytic process. As we know, the active sites are dynamic in real reaction conditions. The morphology evolution and catalytic behavior of the metal nanocluster have close relationship with the structure of the LD materials. Zeng et al. used ab initio molecular dynamics (AIMD) simulations to study the Fe_{53} cluster in contact with either the edge of the graphene nanocavity or graphene nanoribbon to uncover the reaction mechanism of C—C bond-breaking reaction(Figure 10C).[157] They proposed a new reaction mechanism compared to the experiment, called melting recrystallization for the structural transformation of Fe cluster. The AIMD results show that the Fe_{53} cluster undergoes a phase transition from the HCP structure to a liquid-like nanodroplet when supported on monolayer graphene, as shown in Figure 10D. Due to the strong bond between the Fe cluster and the dangling C atoms, Fe_{53} can only catalyze the C—C dissociation at the armchair edge through C—C displacement mechanism (Figure 10E). They also concluded that the catalytic ability of Fe atoms is less efficient than that of Ni atoms because Fe clusters can easily reshape during reaction. Therefore, the control of the morphology of subnanometer atomic clusters in experimental conditions could avoid the loss of reactivity of the catalysts during the reaction process.

7.2. Support and Coordination Effect

LD materials provide excellent platforms for anchoring the single atom and atomic clusters due to their unique structure and electronic properties, such as large surface area, flexible and abundant porous structure and superior electronic conductivity.[6,100,101,170] Different substrates could affect the electronic properties of the active sites and result in different catalytic mechanisms. Figuring out the interaction between the atomic cluster and the substrates could guide the rational design of highly efficient catalysts.[109,171,172] Carbon-based LD materials including graphene,[173–175] graphdiyne (GDY),[176–178] g-C_3N_4,[11,179,180] CN[181–183] and their derivatives have attracted huge interests in designing various electrocatalysts. The electronic properties of atomic clusters could be modified by loading on different substrates. For instance, when small metal clusters supported on the semiconductor substrate, there will be a Mott–Schottky effect at the interface. This effect could stabilize the metal cluster and lead to the ET between the two parts to form a Mott-Schottky barrier. He et al. theoretically demonstrated a Mott-Schottky catalyst composed of a copper trimer and the newly synthesized holey C_2N semiconductor to convert CO into C_3 products.[184] The Mott–Schottky barrier formed at the interface can stabilize the oxidation of Cu_3 cluster and thus significantly boost C—C bond coupling and upgrading that outperforms Cu (1 1 1) and Cu (1 0 0) surfaces. Except for metal atoms catalysts, single non-metal atom catalysts also show unique intrinsic properties that metal atoms do not have. Ling et al. first proposed a metal-free SAC for N_2 fixation (**Figure 11**A).[167] Different from metal atoms, single nonmetal B atom anchored on g-C_3N_4 can act as a "donor-acceptor" active site to activate N≡N bonds and efficiently reduce N_2 into NH_3. In addition, the single B decorated g-C_3N_4 show significantly enhanced visible light absorption, making them ideal for solar-driven reduction of N_2. TM dichalcogenides (TMDs) are other important LD materials for single atom and atomic cluster catalysts because of their variable elemental compositions, flexible electronic structures, diverse crystal structures, and intrinsic activities toward many catalytic reactions.[185] Li et al. reported a single Co atom distributed on 2H-MoS_2 surfaces catalysts for hydrodeoxygenation (HDO) reactions (Figure 11B).[168] DFT calculations show that the formation of metal vacancy interfaces

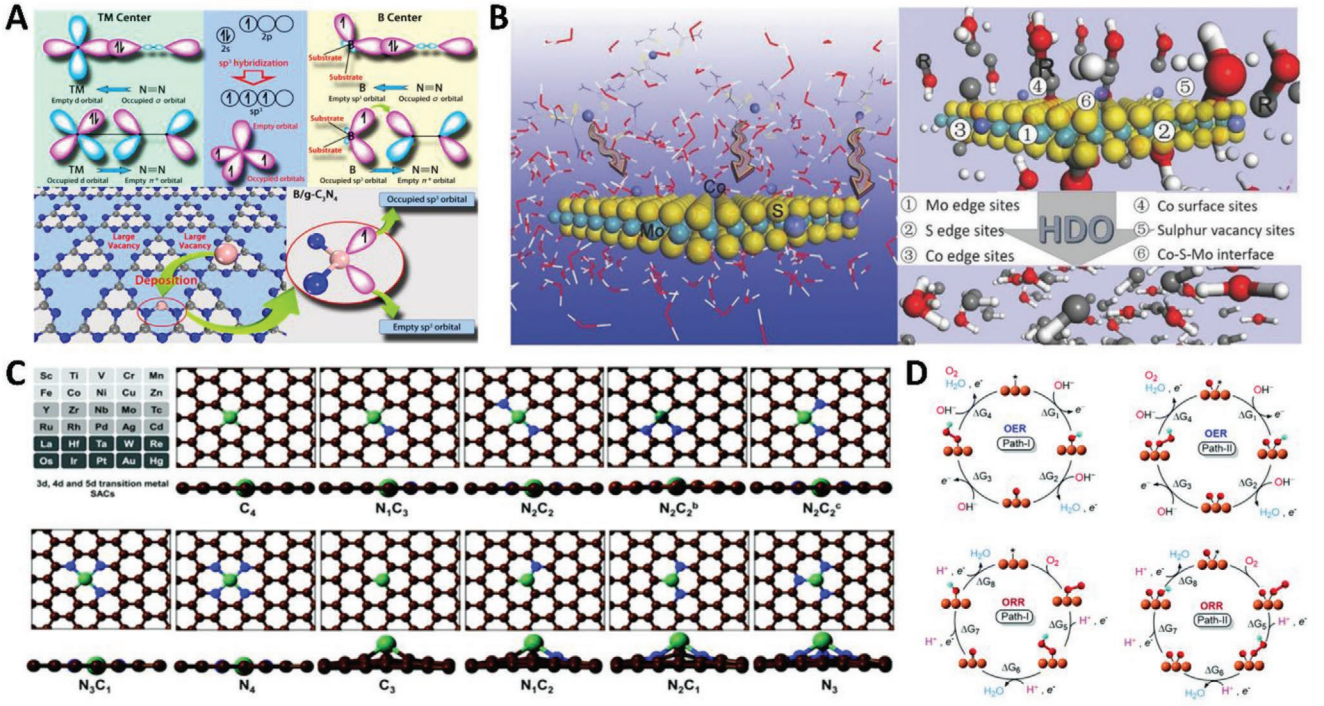

Figure 11. A) Schematic of N_2 activation mechanism on single TM atom and nonmetal B atom. Adapted with permission.[167] Copyright 2018, American Chemical Society. B) Schematic of the Co adsorption on MoS_2 surface in the presence of H_2O and thiourea ligands and possible reaction sites of HDO on Co-MoS_2 catalyst. Adapted with permission.[168] Copyright 2019, Wiley. C) Schematic of a (TM)SA with different coordinations embedded in nitrogen-doped graphene nanosheet. D) Schematic of the different mechanisms and reaction pathways of electrocatalytic reaction cycles on a metal-binding site. Adapted with permission.[169] Copyright 2021, Royal Chemistry Society.

on the MoS_2 surface can promote the H_2 activation on the reactive single Co atom. The TMDs supports can also break scaling relations between adsorption energies of key reaction intermediates that severely limit the catalytic performance of traditional metal surfaces. Li et al. symmetrically studied TM SACs supported on vanadium disulfide (VS_2) for N_2 reduction reaction (NRR).[186] They found strongly broken scaling relations on these SACs for NRR. The reason is attributed to strong charge transfer from single metal atoms to the underlying support which selectively weakens *N and *NH binding strength. Therefore, the supporting effect plays an important role in tuning the catalytic performance.

The coordination environment of single atom and atomic cluster on LD materials can significantly alter the electronic properties of the active sites. Tuning the coordination environment of single atoms to achieve high activity and selectivity is becoming a hot topic in both theoretical[187,188] and experimental[189,190] parts. Ha et al. employed the high-throughput computation and machine learning methods to explore the stability and activity of TM supported on nitrogen-doped graphene (TM–GN) for HER, OER, and ORR.[169] They investigated the formation energy, structural/electrochemical stability, electronic properties, electrical conductivity, and reaction mechanism of 30 single metal atoms anchored on various $-N_nC_m$ moieties to screen out the best combinations for HER, OER, and ORR(Figure 11C). They found that the metal atoms with different coordination could show completely different catalytic performance. A single metal atom with suitable coordination environment can not only improve the activity but also can enhance the stability of the catalysts. Moreover, they demonstrated that the reaction mechanism can be changed by tuning the coordination environment (Figure 11D), which could provide useful guidance on high-performance single-atom catalytic design. This strategy can be also adopted to atomic clusters including metal dimer, triple and small clusters loading on LD materials.

7.3. Microenvironment Effect

The microenvironment around the active site is equally important to the catalytic performance in heterogeneous catalysis community. The confined microenvironment approach on a catalyst, pioneered by Bao et al., has achieved outstanding progress and became an important topic in heterogeneous catalysis.[194] The active stability and chemistry of the active sites can be affected by the confined microenvironment. There are various microenvironments including 0D pores of zeolites, 1D channels of CNTs, and 2D space under 2D materials for confined catalysis (**Figure 12**A).[191] Xiao et al. first theoretically investigated the metal or metal oxide nanoparticles confined inside CNTs.[192] They explored typical TMs such as Fe, FeCo, RhMn, and Ru as models and observed stronger strains and deformations within the CNT channels due to different electronic structures and spatial confinement, which will consequently affect the binding strength of the intermediates on

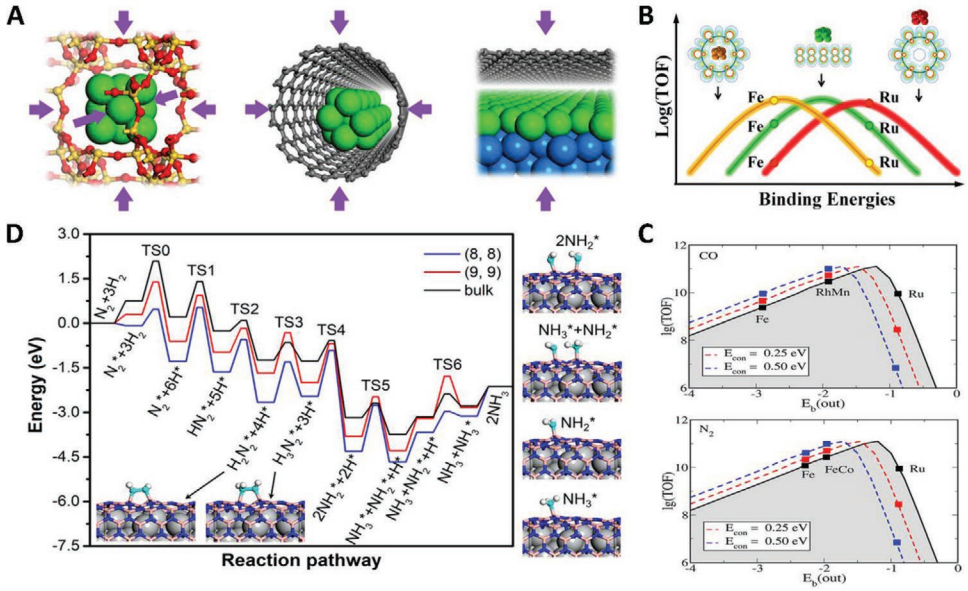

Figure 12. A) Schemes for confined catalysis within various microenvironments. Adapted with permission.[191] Copyright 2017, National Academic of Sciences. B) Schematic of binding energies of CO and N_2 on a variety of catalysts. Adapted with permission.[192] Copyright 2015, American Chemical Society. C) Calculated TOF as a function of the dissociative binding energy. D) Energy diagram of N_2-to-NH_3 conversion on Ti/(8, 8) BNNT, Ti/(9, 9) BNNT, and bulk Ti/h-BN heterostructure. Adapted with permission.[193] Copyright 2019, American Chemical Society.

the active sites. DFT calculations indicated that the volcano curve of the catalytic activities toward the metals with higher binding energies was essentially shifted due to the unique confined environment (Figure 12B). They further calculated the turnover frequencies (TOF) as a function of the dissociative binding energy for CO and N_2 on a variety of catalysts (M = Fe, FeCo, RhMn, and Ru) and found that CO hydrogenation, ammonia synthesis, and decomposition can be well predicted (Figure 12C). Well-defined confined microenvironments could be explored for rational design of efficient catalysts for a much wider range of reactions. He et al. investigated single TM atoms encapsulated in C60 cage structure to act as highly efficient HER catalysts.[195] The inside single metal atom can modulate the surface reactivity of carbon atoms. In a related approach, Zhou et al. encapsulating early TM nanowires into the boron nitride nanotubes (BNNTs) for nitrogen fixation and ammonia synthesis.[193] They use different metals to fill different size of BNNTs. They found that the coexisting occupied and unoccupied p states of B atoms in filled BNNTs can effectively mimic the d states of TM. The B atoms serve as the active sites for associative N_2 adsorption and hydrogenation (Figure 12D). They pointed out that the activity can be optimized by controlling the type of metal filler and size of BN nanotube. The ideal microenvironment surrounding single atom and atomic cluster will result in the modulation of chemical properties of the active sites, and may finally lead to reactions with high activity and selectivity. Strain effect is another important microenvironment on catalysts. Applying different kinds of strain including tensile and compressive strain on active sites could significantly change the catalytic behaviors and can also tune the electronic properties of the catalysts.[196] The sensitivity to mechanical strain of active sites could provide us new pathways to optimize the catalytic performance.[197,198]

8. Electrochemical Energy Devices

Zhang et. al. synthesized a trifunctional electrocatalyst by anchoring cobalt atoms on the nitrogen and sulfur co-doped hollow carbon spheres (CoSA/N,S-HCS) and these catalysts exhibited remarkable electrocatalytic activity and stability for the HER, OER, and ORR.[1] Motivated by the exceptional OER and ORR performance of the as-prepared CoSA/N,S-HCS catalyst, a rechargeable Zn–air battery device was assembled utilizing a gas diffusion layer coated with the CoSA/N,S-HCS catalyst as the air cathode (**Figure 13**A). A mixture of the benchmark Pt/C and RuO_2 electrocatalysts was also examined as the air cathode for the comparison. Figure 13B showed the discharge polarization curves as well as the corresponding power density curves and it is clear from this figure that the CoSA/N,S-HCS catalyst delivers a peak power density (P_{max}) of 173.1 mW cm^{-2} that is significantly higher than the Pt/C + RuO_2 based catalyst (138.8 mW cm^{-2}) and recently reported other SACs for the rechargeable Zn–air batteries.[1] Furthermore, the CoSA/N,S-HCS catalyst-based battery gives a large specific discharge capacity of about 781.1 mAh g^{-1} at a current density of 10 mA cm^{-2} with the corresponding energy density of about 941.1 Wh kg^{-1} according to the consumed Zn mass (Figure 13C), outperforming the Pt/C + RuO_2 catalyst-based battery (712.7 mAh·g^{-1} and 846.7 Wh kg^{-1}, respectively). Also, two Zn–air batteries that are connected in series can lighten an array of 33 yellow light-emitting diodes for several hours (Figure 13C inset).[1] The long-term rechargeability and efficacy of the CoSA/N, S-HCS based battery was also assessed by continuous galvanostatic charge-discharge process at a current density of 10 mA cm^{-2} with 10 min charge and 10 min discharge per cycle. As seen in Figure 13D, the initial voltage gap of the CoSA/N,S-HCS catalyst-based battery is only about 0.82 V, which is superior to

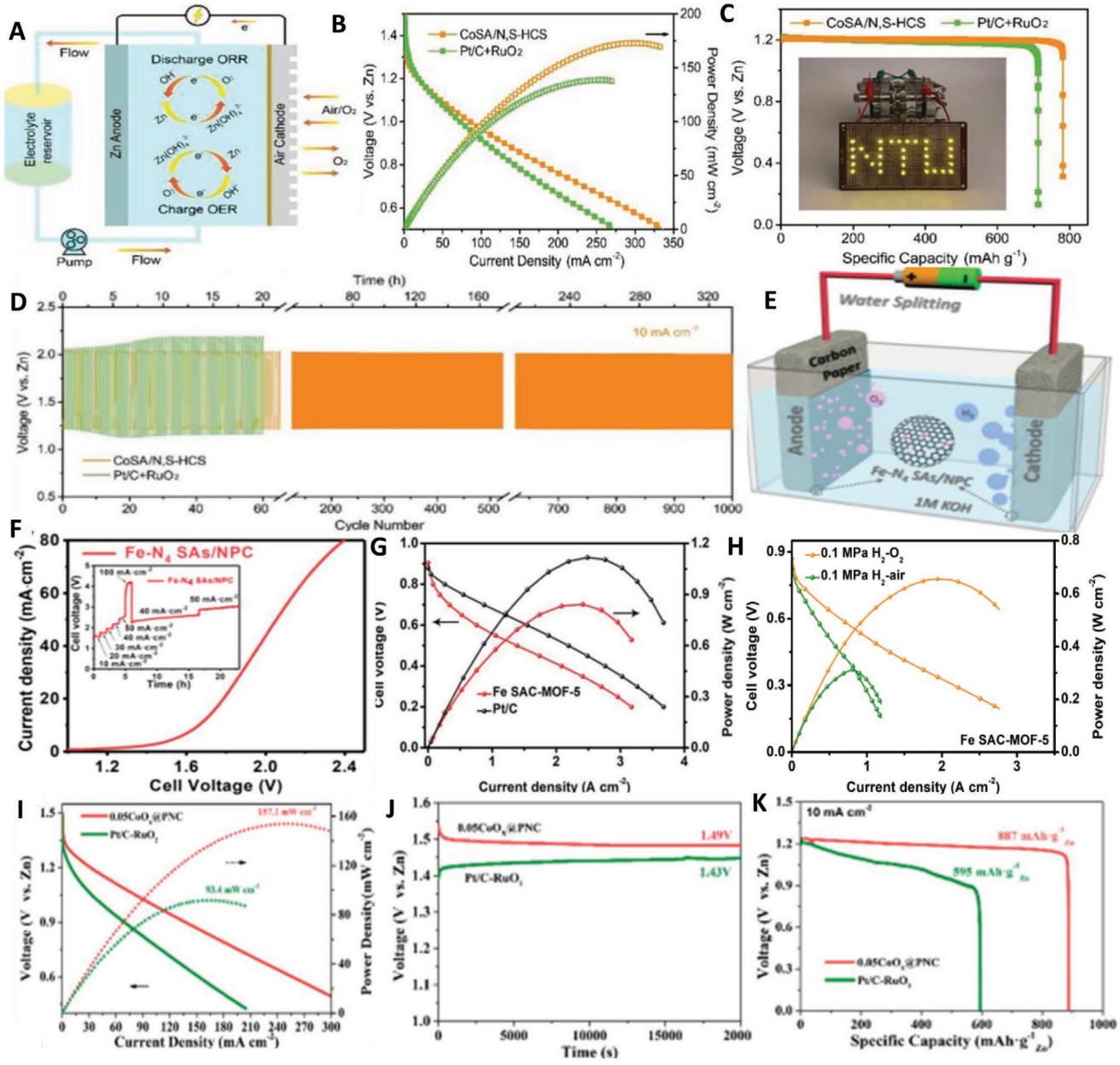

Figure 13. A) Schematic illustration of a Zn–air battery device; B) discharge polarization curves and the corresponding power density plots; C) galvanostatic discharge curves (Inset: a photograph of LEDs powered by tandem liquid batteries); and D) galvanostatic discharge–charge cycling curves of CoSA/N,S-HCS and Pt/C + RuO_2 based Zn–air batteries. Adapted with permission.[199] Copyright 2020, Wiley. E) Schematic illustration of a water-splitting device; and F) LSV curve of the Fe-N_4 SAs/NPC electrodes (Inset: chronopotentiometric curve at different current densities). Adapted with permission.[200] Copyright 2018, Wiley. Fuel cell polarization and power density curves of Fe SAC-MOF-5 cathode catalysts under G) 0.2 MPa H_2–O_2 and H) 0.1 MPa H_2–O_2 and 0.1 MPa H_2–air. Adapted with permission.[203] Copyright 2021, Wiley. I) Discharge polarization curves and the corresponding power density curves; J) open-circuit plots; and K) specific capacities plots at 10 mA cm^{-2} of 0.05 CoO_x@PNC based Zn-air battery devices. Adapted with permission.[202] Copyright 2022, Elsevier.

the benchmark (Pt/C + RuO_2) catalyst-based battery (0.85 V). Notably, a negligible performance fading was observed even after 1000 cycles for the CoSA/N, S-HCS catalyst-based battery, whereas, the voltage gap was sharply increased to 1.04 V after 60 cycles of operation for the (Pt/C + RuO_2) catalyst-based battery. Experimental observations, as well as the theoretical calculations, revealed that the synergistic cooperation between the electron-donating sulfur dopants and atomically dispersed Co—N_4 sites significantly reduced the reaction barriers, thus boosting their electrocatalytic performances for the Zn–air battery devices.[199]

Pan et. al. reported a novel polymerization-pyrolysis-evaporation strategy to prepare nitrogen-doped porous carbon anchored with atomically dispersed iron (Fe-N_4 SAs/NPC) electrocatalysts and they exhibited a great performance towards many electrocatalytic reactions such as HER, OER,

and ORR.[200]2 Encouraged by the remarkable tri-functional HER, OER, and ORR performances of the as-synthesized Fe-N_4 SAs/NPC electrocatalyst, they constructed a water electrolyzer device (Figure 13E) to test their practical applicability. For the overall water-splitting reaction, the Fe-N_4 SAs/NPC electrocatalyst just needs a lower potential of about 1.67 V to reach a current density of 10 mA cm^{-2} (Figure 13F). Furthermore, it also showed an outstanding long-term stability performance during the 23 h of operation period (inset of Figure 13F).

Xie et. al. synthesized ultrahigh porous carbon using a metal–organic framework namely MOF-5 as a precursor and used this carbon as an efficient support to prepare iron SACs (Fe SAC-MOF-5).[201] This Fe SAC-MOF-5 electrocatalyst delivered a halfwave potential ($E_{1/2}$) of 0.83 V in a 0.5 M sulfuric acid electrolyte solution, demonstrating their remarkable performance for the ORR reactions. Inspiring from this outstanding ORR performance, they also tested their performance in the proton exchange membrane fuel cells (PEMFCs). The H_2–O_2 fuel cell device was assembled utilizing Fe SAC-MOF-5 electrocatalyst as the cathode material (4 mg cm^{-2}) for the ORR process and PtRu/C electrocatalyst as the anode material for the hydrogen oxidation reaction (HOR).[201] Under the H_2–O_2 conditions (0.2 MPa pressure for O_2), the open-circuit voltage was found to be 0.90 V for the Fe SAC-MOF-5 (Figure 13G), which was even higher than that of the benchmark Pt/C catalyst (0.88 V). The peak power density (P_{max}) is considered an important standard for assessing the performance of an electrocatalyst under the real working conditions. The as-prepared iron SAC-based H_2–O_2 fuel cells attained a P_{max} of 0.65 and 0.84 W cm^{-2} under 0.1 and 0.2 MPa, respectively, outperforming most of reported PEMFCs constructed with SACs. Fe SAC-MOF-5 catalyst was also evaluated under 0.1 MPa H_2–air condition and attained a P_{max} of 0.31 W cm^{-2} (Figure 13H). This outstanding performance generates from the ultrahigh specific surface area of the as-synthesized carbon from MOF-5 for the construction of a high density of metallic single iron atoms as well as higher external surface area for the improved exposure of the available electroactive sites.

Tan et al. introduced a novel microporous metal–organic framework confinement strategy to confine sub-nanometer CoO_x clusters into the small pores of ZIF-8 MOF-derived N-doped carbon nanomaterials (0.05CoO_x@PNC) and they displayed outstanding bifunctional activity towards the OER and ORR reactions.[202] In view of the excellent bifunctional activity of the 0.05CoO_x@PNC cluster catalysts, a rechargeable zinc-air battery was constructed using 0.05CoO_x@PNC as air cathode. As seen in Figure 13I, the 0.05CoO_x@PNC catalyst-based zinc-air battery device achieved a high peak power density of about 157.1 mW cm^{-2} than that of the Pt/C-RuO_2-based device (mW cm^{-2}). Additionally, the prepared zinc-air battery with 0.05CoO_x@PNC cluster catalyst exhibited a higher open-circuit voltage of about 1.49 V that is higher than the (Pt/C-RuO_2) catalyst-based zinc–air battery (1.43 V) (Figure 13J). Furthermore, the 0.05CoO_x@PNC cluster electrocatalyst also delivered a higher specific capacity of about 887 mAh·g_{Zn}^{-1} at a current density of 10 mA cm^{-2} (Figure 13K) with an energy density of about 1020 Wh·kg_{Zn}^{-1}, which surpasses Pt/C-RuO_2 (595 mAh·g_{Zn}^{-1} and 541 Wh·kg_{Zn}^{-1}, respectively). Theoretical calculations revealed that the reducing particle size, as well as the coupling with the Co-N, could efficiently regulate the charge distribution of the CoO_x nanoclusters, downshifting the D-band center of the Co adsorption sites in the CoO_x nanoclusters, which reduced the reaction barrier of the intermediate catalytic species and improve the overall electrocatalytic activities.

H_2/CO_2 fuel cells have recently sparked a tremendous interest among the scientific community due to their unique capabilities to utilize CO_2 as a unique resource to obtain electricity while producing valuable fuels.[204] In a typical H_2/CO_2 fuel cell, H_2 and CO_2 are consumed via HOR and CO_2RR reactions into the anode and cathode, respectively. Nevertheless, as a technology that is just in its initial stages, the electrocatalytic rates of the CO_2 reduction are decisively controlled by cathode catalysts. Owed to the poor reactivity and high thermodynamic stability of CO_2 molecules, the development of highly efficient CO_2RR electrocatalysts is crucial to enhance the performance of H_2/CO_2 fuel cells. In this regards, Yongning Liu and coworkers have successfully functionalized N-doped carbon nanofibers with Ru atomic clusters (Ru-CNFs) in order to fabricate ultraefficient cathodes for H_2/CO_2 fuel cells (**Figure 14**A).[205] The polarization and power density curves of the H_2/CO_2 fuel cell were studied at different operating temperatures (Figure 14B). Remarkably, the cell delivered a maximum power density of 0.25 W m^{-2} at 80 °C. Although HER fulfilled a key role in the generation of electricity in the fuel cell, the production of CH_4 reached a maximum value at 170 °C, thus demonstrating a high selectivity at higher temperatures of the Ru-CNF catalysts toward the production of CH_4 fuel (Figure 14C). These findings provide a strong platform to fabricate carbon-based heterostructure nanomaterials as efficient cathodes for H_2/CO_2 fuel cells.

Among the most promising renewable energy technologies, microbial fuel cells (MFC) are emerging as a green strategy to effectively trigger the degradation of organic pollutants in wastewater samples while producing electrons.[206,207] In a typical MFC, electricigenic bacteria on the anode decompose the organic materials in wastewater into CO_2 and H_2O while generating electrons. These electrons are transferred to cathode via an external circuit to be enrolled in an ORR. Zhang and coworkers have designed, via mechanochemical synthesis, iron-based clusters embedded into nitrogen-doped activate carbon (Fe-clusters/NAC) as superior electrocatalysts for MFC cathodes.[208] Abiotic electrochemical tests were conducted to evaluate the ORR performance of AC, NAC, Fe-clusters/NAC, and commercial Pt catalysts (Figure 14D,E). Fe-clusters/NAC catalysts rendered the more efficient electrochemical performance delivering a current density of 56.2 A m^{-2} of Fe-clusters/NAC catalysts at 0.16 V versus SHE, which are much higher than those of Pt (37.2 A m^{-2}), NAC (35.9 A m^{-2}) and AC (20.0 A m^{-2}). The power density of the Fe-clusters/NAC catalysts-based MFCs reached 2387 mW m^{-2}, which is the highest value among all the reported Fe—N—C catalysts under the same experimental parameters (Figure 14F). This work highlight the key role of quaternary N and Fe—N active sites to develop superior MFCs.

Fe—Co dimers embedded in nitrogen-doped carbon networks have been used to create active sites for ORR under acidic conditions as cathodic catalysts for H_2/O_2 fuel cells.[209] The outstanding power density and long-term stability values

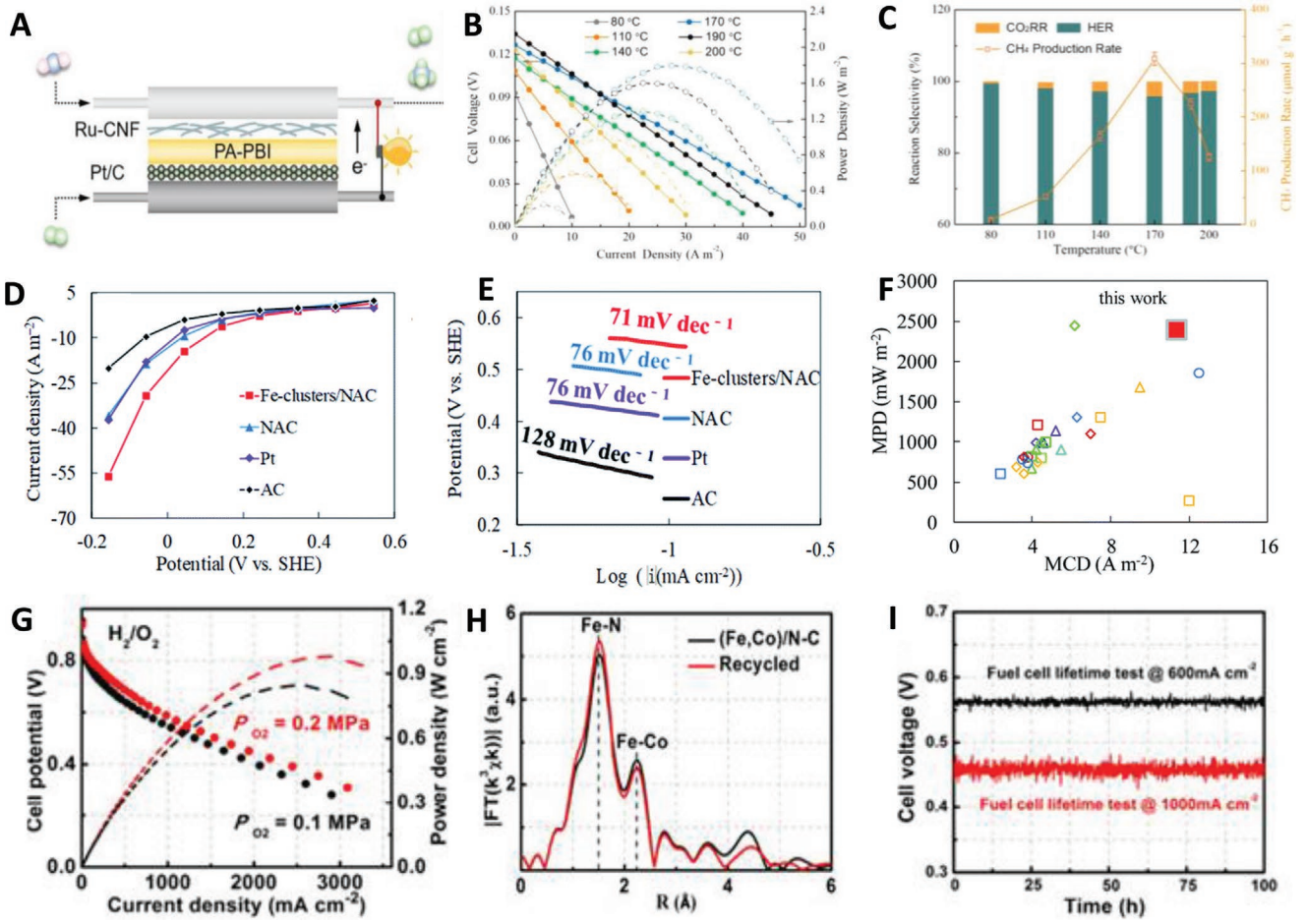

Figure 14. A) Schematic illustration of the H_2/CO_2 fuel cell. B) Polarization and power density curves of the H_2/CO_2 fuel cell. C) Cathodic reaction selectivity for CO_2RR and the HER, and the corresponding production rates for CH_4 at different temperatures from 80 to 200 °C. Adapted with permission.[205] Copyright 2021, American Chemical Society. D) Current–potential curves in abiotic electrochemical cells based on chronoamperometry tests. E) Tafel plots of the Fe ACEs. F) Comparison of the Fe-clusters/NAC catalysts with other Fe/NC catalysts reported in the last five years. Adapted with permission.[208] Copyright 2020, Royal Chemistry Society. G) H_2/O_2 fuel cell polarization plots. Cathode: ≈0.77 mg cm^{-2} of (Fe,Co)/N−C; 100% RH; O2, 0.1, and 0.2 MPa partial pressures. Anode: 0.1 mgPt cm^{-2} Pt/C; 100% RH;H2, 0.1 MPa partial pressure, cell 353 K; 25 cm^2 electrode area. H) Fe K-edge EXAFS fitting curves of (Fe,Co)/N-C and (Fe,Co)/N-C electrocatalysts after stability test. I) Stability measurement of (Fe,Co)/N-C in an H_2/air fuel cell at 600 mA cm^{-2} and 1000 and mA cm^{-2}. Adapted with permission.[209] Copyright 2017, American Chemical Society.

revealed its potential in lowering the gap between nonprecious dual-atom Fe-Co catalysts and commercial Pt-based catalysts (Figure 14G–I).

9. Concluding Remarks and Future Prospects

Single atom and atomic cluster catalysts became in the last years the frontier of heterogeneous catalysis due to their possibility to exhibit unusual reactivity and selectivity. As we have shown, a lot of breakthroughs in the synthesis of SACs and ACEs via confinement, defect engineering, and coordination strategy, have been recently accomplished. The development of powerful characterization techniques, especially in situ-electrochemical techniques, have allowed researchers to track the real-time dynamic structure evolution of low-nuclearity electrocatalysts, thus promoting the determination of real active sites and plausible catalytic pathways.

Despite all the experimental advances in the development of SACs and ACEs, some key drawbacks have remained elusive. The accurate control of the local environment of metallic centers should be notably improved to decrease the aggregation phenomena by the proper selection of precursors and supports together with the development of more efficient synthetic methodologies. Furthermore, additional new characterization methods must be developed to unlock the dynamic interactions between the active sites and catalytic intermediates in order to provide an in-depth understanding on the path of multistep electrocatalytic reactions.

The overarching aim to understand the structure-property relationship and achieve the computational design of high-performance electrocatalysts that boost the time-consuming trial-and-error process will be done with the aid of state-of-the-art theoretical simulation. However, the current gap between the experiment and theory is still a pending task that needs to be carefully addressed. First, the difference between simulation

models and the real catalysts is the main reason that leads to the inaccurate predictions. Most of the theoretical work on single atom or atomic cluster catalysts can only predict the trends of the catalytic performance. The structures of the catalysts are usually very complex while the constructed simulation models can not accurately reflect the catalytic activity of real catalysts. Second, the diverse and complicated reaction conditions are very hard to fully consider in the simulation and will also be extremely expensive for computations. To narrow down the gaps, the rapid development of multi-scale simulation and machine-learning methods and the synergy of theory and experiment will be powerful tools to certainly accelerate the development of highly efficient catalysts for a myriad of energy-related applications.

Acknowledgements

T.H., A.R.P.-S., and S.X. contributed equally to the work. The publication have been supported by RUDN Strategic Academic Leadership Program (R. Luque). Additionally, this publication has been supported by the President's International Fellowship Initiative for visiting scientists of the Chinese Academy of Sciences. Prof. Guobao Xu acknowledges the National Natural Science Foundation of China (Nos. 22174136 and 21874126).

Conflict of Interest

The authors declare no conflict of interest.

Keywords

electrochemical devices, energy conversion, low-dimensional nanomaterials, low nuclearity catalysts

Received: February 9, 2022
Revised: March 22, 2022
Published online:

[1] M. A. Ahsan, T. He, J. C. Noveron, K. Reuter, A. R. Puente-Santiago, R. Luque, *Chem. Soc. Rev.* **2022**, *51*, 812.
[2] N. D. Popovich, D. Rajagopal, E. Tasar, A. Phadke, *Nat. Energy* **2021**, *6*, 1017.
[3] P. Trogadas, M.-O. Coppens, *Chem. Soc. Rev.* **2020**, *49*, 3107.
[4] Y. Shi, Z. Lyu, M. Zhao, R. Chen, Q. N. Nguyen, Y. Xia, *Chem. Rev.* **2020**, *121*, 649.
[5] C. Edmund, C. J. Barile, N. A. Kirchschlager, Y. Li, J. P. Gewargis, S. C. Zimmerman, A. Hosseini, A. A. Gewirth, *Nat. Mater.* **2016**, *15*, 754.
[6] D. Zhao, Z. Zhuang, X. Cao, C. Zhang, Q. Peng, C. Chen, Y. Li, *Chem. Soc. Rev.* **2020**, *49*, 2215.
[7] S. Mitchell, J. Pérez-Ramírez, *Nat. Rev. Mater.* **2021**, *6*, 969.
[8] J. Cai, R. Javed, D. Ye, H. Zhao, J. Zhang, *J. Mater. Chem. A* **2020**, *8*, 22467.
[9] S. Mitchell, R. Qin, N. Zheng, J. Pérez-Ramírez, *Nat. Nanotechnol.* **2021**, *16*, 129.
[10] S. K. Kaiser, Z. Chen, D. Faust Akl, S. Mitchell, J. Pérez-Ramírez, *Chem. Rev.* **2020**, *120*, 11703.
[11] T. He, C. Zhang, L. Zhang, A. Du, *Nano Res.* **2019**, *12*, 1817.
[12] H. Rong, S. Ji, J. Zhang, D. Wang, Y. Li, *Nat. Commun.* **2020**, *11*, 1.
[13] X. Li, H. Rong, J. Zhang, D. Wang, Y. Li, *Nano Res.* **2020**, *13*, 1842.
[14] Y. Wang, Y. Zheng, C. Han, W. Chen, *Nano Res.* **2021**, *14*, 1682.
[15] C. Tang, L. Chen, H. Li, L. Li, Y. Jiao, Y. Zheng, H. Xu, K. Davey, S.-Z. Qiao, *J. Am. Chem. Soc.* **2021**, *143*, 7819.
[16] Y. Fan, S. Liu, Y. Yi, H. Rong, J. Zhang, *ACS Nano* **2021**, *15*, 2005.
[17] C.-C. Hou, H.-F. Wang, C. Li, Q. Xu, *Energy Environ. Sci.* **2020**, *13*, 1658.
[18] X. Ren, J. Li, S. Wang, D. Zhang, Y. Wang, *Catal. Commun.* **2019**, *128*, 105709.
[19] M. J. Wang, M. Ji, X. Zheng, C. Jiang, H. Zhao, Z. X. Mao, M. Zhang, C. Zhu, J. Xu, *Appl. Surf. Sci.* **2021**, *551*, 148742.
[20] S. Bai, F. Liu, B. Huang, F. Li, H. Lin, T. Wu, M. Sun, J. Wu, Q. Shao, Y. Xu, X. Huang, *Nat. Commun.* **2020**, *11*, 954.
[21] J. Di, C. Chen, S.-Z. Yang, S. Chen, M. Duan, J. Xiong, C. Zhu, R. Long, W. Hao, Z. Chi, H. Chen, Y.-X. Weng, J. Xia, L. Song, S. Li, H. Li, Z. Liu, *Nat. Commun.* **2019**, *10*, 2840.
[22] H. Zhang, S. Sui, X. Zheng, R. Cao, P. Zhang, *Appl. Catal., B* **2019**, *257*, 117878.
[23] S. Ni, H. Zhang, Y. Zhao, X. Li, Y. Sun, J. Qian, Q. Xu, P. Gao, D. Wu, K. Kato, M. Yamauchi, Y. Sun, *Chem. Eng. J.* **2019**, *366*, 631.
[24] X. Liao, J. Hou, Y. Wang, H. Zhang, Y. Sun, X. Li, S. Tang, K. Kato, M. Yamauchi, Z. Jiang, *Green Chem.* **2019**, *21*, 4194.
[25] Z. Zhang, J. Liu, J. Wang, Q. Wang, Y. Wang, K. Wang, Z. Wang, M. Gu, Z. Tang, J. Lim, T. Zhao, F. Ciucci, *Nat. Commun.* **2021**, *12*, 5235.
[26] Y. Ma, X. Zhang, L. Cao, J. Lu, *Catal. Sci. Technol.* **2021**, *11*, 2844.
[27] W. Liu, Q. Su, L. Yu, G. Du, C. Li, M. Zhang, S. Ding, B. Xu, *J. Alloys Compd.* **2021**, *886*, 161189.
[28] J. Chen, L. Chen, X. Wang, Z. Rao, J. Sun, A. Chen, X. Xie, *J. Colloid Interface Sci.* **2022**, *605*, 674.
[29] J. H. Kwak, J. Hu, D. Mei, C.-W. Yi, D. H. Kim, C. H. F. Peden, L. F. Allard, J. Szanyi, *Science* **2009**, *325*, 1670.
[30] Z. Zeng, Y. Su, X. Quan, W. Choi, G. Zhang, N. Liu, B. Kim, S. Chen, H. Yu, S. Zhang, *Nano Energy* **2020**, *69*, 104409.
[31] L.-Q. Yu, W.-J. Xia, W.-J. Ma, T.-E. Wen, S.-L. Chen, F. Jin, B.-C. Huang, R.-C. Jin, *ACS Appl. Mater. Interfaces* **2021**, *13*, 13534.
[32] W. Liu, W. Hu, L. Yang, J. Liu, *Nano Energy* **2020**, *73*, 104750.
[33] S. Ding, H.-A. Chen, O. Mekasuwandumrong, M. J. Hülsey, X. Fu, Q. He, J. Panpranot, C.-M. Yang, N. Yan, *Appl. Catal., B* **2021**, *281*, 119471.
[34] S. Jin, Y. Ni, Z. Hao, K. Zhang, Y. Lu, Z. Yan, Y. Wei, Y.-R. Lu, T.-S. Chan, J. Chen, *Angew. Chem., Int. Ed.* **2020**, *59*, 21885.
[35] Y. Cheng, S. Zhao, B. Johannessen, J.-P. Veder, M. Saunders, M. R. Rowles, M. Cheng, C. Liu, M. F. Chisholm, R. De Marco, H.-M. Cheng, S.-Z. Yang, S. P. Jiang, *Adv. Mater.* **2018**, *30*, 1706287.
[36] E. Zhang, T. Wang, K. Yu, J. Liu, W. Chen, A. Li, H. Rong, R. Lin, S. Ji, X. Zheng, *J. Am. Chem. Soc.* **2019**, *141*, 16569.
[37] D. Liu, C. Wu, S. Chen, S. Ding, Y. Xie, C. Wang, T. Wang, Y. A. Haleem, Z. ur Rehman, Y. Sang, Q. Liu, X. Zheng, Y. Wang, B. Ge, H. Xu, L. Song, *Nano Res.* **2018**, *11*, 2217.
[38] Z. Cai, P. Du, W. Liang, H. Zhang, P. Wu, C. Cai, Z. Yan, *J. Mater. Chem. A* **2020**, *8*, 15012.
[39] H. Rong, L. Meng, E. Zhang, H. Peng, Y. Wang, D. Wang, J. Zhang, *ChemCatChem.*
[40] Y. Liu, B. Huang, X. Zhang, X. Huang, Z. Xie, *J. Power Sources* **2019**, *412*, 125.
[41] N. Xuan, J. Chen, J. Shi, Y. Yue, P. Zhuang, K. Ba, Y. Sun, J. Shen, Y. Liu, B. Ge, Z. Sun, *Chem. Mater.* **2019**, *31*, 429.
[42] H. Shin, W.-G. Jung, D.-H. Kim, J.-S. Jang, Y. H. Kim, W.-T. Koo, J. Bae, C. Park, S.-H. Cho, B. J. Kim, I.-D. Kim, *ACS Nano* **2020**, *14*, 11394.
[43] J. Y. Jung, J.-H. Jang, J.-G. Kim, K.-S. Lee, H.-K. Lim, P. Kim, R. P. H. Chang, J.-W. Park, S. J. Yoo, N. D. Kim, *Small Methods* **2021**, *5*, 2100239.
[44] A. A. Topalov, S. Cherevko, A. R. Zeradjanin, J. C. Meier, I. Katsounaros, K. J. J. Mayrhofer, *Chem. Sci.* **2014**, *5*, 631.

[45] Z. Chen, C. Liu, J. Liu, J. Li, S. Xi, X. Chi, H. Xu, I.-H. Park, X. Peng, X. Li, W. Yu, X. Liu, L. Zhong, K. Leng, W. Huang, M. J. Koh, K. P. Loh, *Adv. Mater.* **2020**, *32*, 1906437.
[46] J. Liu, C. Cao, X. Liu, L. Zheng, X. Yu, Q. Zhang, L. Gu, R. Qi, W. Song, *Angew. Chem., Int. Ed.* **2021**, *60*, 15248.
[47] X. Ge, G. Su, W. Che, J. Yang, X. Zhou, Z. Wang, Y. Qu, T. Yao, W. Liu, Y. Wu, *ACS Catal.* **2020**, *10*, 10468.
[48] K. Liu, X. Zhao, G. Ren, T. Yang, Y. Ren, A. F. Lee, Y. Su, X. Pan, J. Zhang, Z. Chen, J. Yang, X. Liu, T. Zhou, W. Xi, J. Luo, C. Zeng, H. Matsumoto, W. Liu, Q. Jiang, K. Wilson, A. Wang, B. Qiao, W. Li, T. Zhang, *Nat. Commun.* **2020**, *11*, 1263.
[49] N. Zhang, X. Zhang, L. Tao, P. Jiang, C. Ye, R. Lin, Z. Huang, A. Li, D. Pang, H. Yan, Y. Wang, P. Xu, S. An, Q. Zhang, L. Liu, S. Du, X. Han, D. Wang, Y. Li, *Angew. Chem., Int. Ed.* **2021**, *60*, 6170.
[50] C. Zhao, Y. Wang, Z. Li, W. Chen, Q. Xu, D. He, D. Xi, Q. Zhang, T. Yuan, Y. Qu, J. Yang, F. Zhou, Z. Yang, X. Wang, J. Wang, J. Luo, Y. Li, H. Duan, Y. Wu, Y. Li, *Joule* **2019**, *3*, 584.
[51] Y. Zhou, J. Li, X. Gao, W. Chu, G. Gao, L.-W. Wang, *J. Mater. Chem. A* **2021**, *9*, 9979.
[52] H. Song, R. Du, Y. Wang, D. Zu, R. Zhou, Y. Cai, F. Wang, Z. Li, Y. Shen, C. Li, *Appl. Catal., B* **2021**, *286*, 119898.
[53] Y. Luo, S. Zhang, H. Pan, S. Xiao, Z. Guo, L. Tang, U. Khan, B.-F. Ding, M. Li, Z. Cai, Y. Zhao, W. Lv, Q. Feng, X. Zou, J. Lin, H.-M. Cheng, B. Liu, *ACS Nano* **2020**, *14*, 767.
[54] J.-C. Li, D.-M. Tang, P.-X. Hou, G.-X. Li, M. Cheng, C. Liu, H.-M. Cheng, *MRS Commun.* **2018**, *8*, 1158.
[55] D. Cao, J. Wang, H. Xu, D. Cheng, *Small* **2021**, *17*, 2101163.
[56] J. Lin, Y. Chen, Y. Zhou, L. Li, B. Qiao, A. Wang, J. Liu, X. Wang, T. Zhang, *AIChE J.* **2017**, *63*, 4003.
[57] R. Jin, M. Peng, A. Li, Y. Deng, Z. Jia, F. Huang, Y. Ling, F. Yang, H. Fu, J. Xie, *J. Am. Chem. Soc.* **2019**, *141*, 18921.
[58] X. Gao, G. Yu, L. Zheng, C. Zhang, H. Li, T. Wang, P. An, M. Liu, X. Qiu, W. Chen, W. Chen, *ACS Appl. Energy Mater.* **2019**, *2*, 966.
[59] L. Cheng, Y. Li, A. Chen, Y. Zhu, C. Li, *Chem. - Asian J.* **2019**, *14*, 2112.
[60] S. Zhang, H. Gao, Y. Huang, X. Wang, T. Hayat, J. Li, X. Xu, X. Wang, *Environ. Sci.: Nano* **2018**, *5*, 1179.
[61] H. Guan, J. Lin, L. Li, X. Wang, T. Zhang, *Appl. Catal., B* **2016**, *184*, 299.
[62] X. Yu, J. Guo, B. Li, J. Xu, P. Gao, K. S. Hui, K. N. Hui, H. Shao, *ACS Appl. Mater. Interfaces* **2021**, *13*, 26891.
[63] J. Si, S. Xiao, Y. Wang, L. Zhu, X. Xia, Z. Huang, Y. Gao, *Nanoscale* **2018**, *10*, 2596.
[64] Q. Hu, Z. Han, X. Wang, G. Li, Z. Wang, X. Huang, H. Yang, X. Ren, Q. Zhang, J. Liu, C. He, *Angew. Chem., Int. Ed.* **2020**, *59*, 19054.
[65] N. Wang, Q. Sun, T. Zhang, A. Mayoral, L. Li, X. Zhou, J. Xu, P. Zhang, J. Yu, *J. Am. Chem. Soc.* **2021**, *143*, 6905.
[66] X. Chen, M. Peng, X. Cai, Y. Chen, Z. Jia, Y. Deng, B. Mei, Z. Jiang, D. Xiao, X. Wen, N. Wang, H. Liu, D. Ma, *Nat. Commun.* **2021**, *12*, 2664.
[67] K. Sonobe, M. Tanabe, K. Yamamoto, *ACS Nano* **2020**, *14*, 1804.
[68] W. Wang, S. Xi, Y. Shao, X. Gao, J. Lin, C. Meng, W. Wang, X. Guo, G. Li, *ChemElectroChem* **2019**, *6*, 1846.
[69] Y. Lu, W. Chen, *Chem. Soc. Rev.* **2012**, *41*, 3594.
[70] K. Yamamoto, T. Imaoka, M. Tanabe, T. Kambe, *Chem. Rev.* **2020**, *120*, 1397.
[71] T. Tsukamoto, T. Kambe, A. Nakao, T. Imaoka, K. Yamamoto, *Nat. Commun.* **2018**, *9*, 3873.
[72] P. Qiu, Y. Yao, W. Li, Y. Sun, Z. Jiang, B. Mei, L. Gu, Q. Zhang, T. Shang, X. Yu, J. Yang, Y. Fang, G. Zhu, Z. Zhang, X. Zhu, T. Zhao, W. Jiang, Y. Fan, L. Wang, B. Ma, L. Liu, Y. Yu, W. Luo, *Nano Lett.* **2021**, *21*, 700.
[73] J. Wojciechowska, E. Gitzhofer, J. Grams, A. M. Ruppert, N. Keller, *Materials* **2018**, *11*, 2329.
[74] K. Wenderich, G. Mul, *Chem. Rev.* **2016**, *116*, 14587.
[75] J. Si, L. Yu, Y. Wang, Z. Huang, K. Homewood, Y. Gao, *Appl. Surf. Sci.* **2020**, *511*, 145577.
[76] J. Zhao, J. Liu, C. Jin, F. Wang, *ACS Appl. Mater. Interfaces* **2021**, *13*, 8395.
[77] J. Wojciechowska, E. Gitzhofer, J. Grams, A. M. Ruppert, N. Keller, *Catal. Today* **2019**, *326*, 8.
[78] L. Zhu, Y. Wu, S. Wu, F. Dong, J. Xia, B. Jiang, *ACS Appl. Mater. Interfaces* **2021**, *13*, 9216.
[79] Q. Cheng, C. Hu, G. Wang, Z. Zou, H. Yang, L. Dai, *J. Am. Chem. Soc.* **2020**, *142*, 5594.
[80] J. Yang, W. Fu, C. Chen, W. Chen, W. Huang, R. Yang, Q. Kong, B. Zhang, J. Zhao, C. Chen, J. Luo, F. Yang, X. Duan, Z. Jiang, Y. Qin, *ACS Catal.* **2021**, *11*, 4146.
[81] Z. Yang, S. Zhang, H. Zhao, A. Li, L. Luo, L. Guo, *ACS Catal.* **2021**, *11*, 11542.
[82] Z. Kou, W. Zang, Y. Ma, Z. Pan, S. Mu, X. Gao, B. Tang, M. Xiong, X. Zhao, A. K. Cheetham, L. Zheng, J. Wang, *Nano Energy* **2020**, *67*, 104288.
[83] H. C. Choi, M. Shim, S. Bangsaruntip, H. Dai, *J. Am. Chem. Soc.* **2002**, *124*, 9058.
[84] C.-Y. Chang, A. Kashale, C.-M. Lee, S.-L. Chu, Y.-F. Lin, I. P. Chen, *Mater. Today Energy* **2021**, *20*, 100693.
[85] Y. Cheng, S. Zhao, B. Johannessen, J. P. Veder, M. Saunders, M. R. Rowles, M. Cheng, C. Liu, M. F. Chisholm, R. De Marco, *Adv. Mater.* **2018**, *30*, 1706287.
[86] Y. Xue, B. Huang, Y. Yi, Y. Guo, Z. Zuo, Y. Li, Z. Jia, H. Liu, Y. Li, *Nat. Commun.* **2018**, *9*, 1.
[87] L. Wang, L. Huang, F. Liang, S. Liu, Y. Wang, H. Zhang, *Chin. J. Catal.* **2017**, *38*, 1528.
[88] Z. Pu, I. S. Amiinu, R. Cheng, P. Wang, C. Zhang, S. Mu, W. Zhao, F. Su, G. Zhang, S. Liao, *Nano-Micro Lett.* **2020**, *12*, 1.
[89] L. Li, X. Chang, X. Lin, Z.-J. Zhao, J. Gong, *Chem. Soc. Rev.* **2020**, *49*, 8156.
[90] Y. Wang, D. Wang, Y. Li, *Adv. Mater.* **2021**, *33*, 2008151.
[91] X. Cao, D. Tan, B. Wulan, K. Hui, K. Hui, J. Zhang, *Small Methods* **2021**, *5*, 2100700.
[92] Y. Zou, S. Wang, *Adv. Sci.* **2021**, *8*, 2003579.
[93] Y. Zhu, T.-R. Kuo, Y.-H. Li, M.-Y. Qi, G. Chen, J. Wang, Y.-J. Xu, H. M. Chen, *Energy Environ. Sci.* **2021**, *14*, 1928.
[94] L. Jiao, W. Xu, Y. Wu, H. Yan, W. Gu, D. Du, Y. Lin, C. Zhu, *Chem. Soc. Rev.* **2021**, *50*, 750.
[95] L. Yang, J. Shui, L. Du, Y. Shao, J. Liu, L. Dai, Z. Hu, *Adv. Mater.* **2019**, *31*, 1804799.
[96] J. Liu, H. Zhang, M. Qiu, Z. Peng, M. K. Leung, W.-F. Lin, J. Xuan, *J. Mater. Chem. A* **2020**, *8*, 2222.
[97] Y. N. Chen, X. Zhang, Z. Zhou, *Small Methods* **2019**, *3*, 1900050.
[98] J. Zhang, Z. Xia, L. Dai, *Sci. Adv.* **2015**, *1*, e1500564.
[99] H. Zhao, C. Zhang, H. Li, J. Fang, *Nano Sel.* **2021**, *2*, 2072.
[100] Y. Wang, J. Mao, X. Meng, L. Yu, D. Deng, X. Bao, *Chem. Rev.* **2018**, *119*, 1806.
[101] T. He, Y. Kong, A. R. P. Santiago, M. A. Ahsan, H. Pan, A. Du, *Mater. Chem. Front.* **2021**, *5*, 6392.
[102] T. He, C. Tang, A. R. P. Santiago, R. Luque, H. Pan, A. Du, *J. Mater. Chem. A* **2021**, *9*, 13192.
[103] A. R. Puente Santiago, M. F. Sanad, A. Moreno-Vicente, M. A. Ahsan, M. R. Cerón, Y.-R. Yao, S. T. Sreenivasan, A. Rodriguez-Fortea, J. M. Poblet, L. Echegoyen, *J. Am. Chem. Soc.* **2021**, *143*, 6037.
[104] X. Wang, S. Qiu, J. Feng, Y. Tong, F. Zhou, Q. Li, L. Song, S. Chen, K. H. Wu, P. Su, *Adv. Mater.* **2020**, *32*, 2004382.
[105] X. K. Wan, H. B. Wu, B. Y. Guan, D. Luan, X. W. Lou, *Adv. Mater.* **2020**, *32*, 1901349.
[106] A. Pedersen, J. Barrio, A. Li, R. Jervis, D. J. Brett, M. M. Titirici, I. E. Stephens, *Adv. Energy Mater.* **2022**, *12*, 2102715.

[107] Y. Wang, F.-L. Hu, Y. Mi, C. Yan, S. Zhao, *Chem. Eng. J.* **2021**, *406*, 127135.
[108] S. Lin, H. Xu, Y. Wang, X. C. Zeng, Z. Chen, *J. Mater. Chem. A* **2020**, *8*, 5663.
[109] T. He, A. R. P. Santiago, Y. Kong, M. A. Ahsan, R. Luque, A. Du, H. Pan, *Small* **2021**, *18*, 2106091.
[110] J. Wang, H. Kong, J. Zhang, Y. Hao, Z. Shao, F. Ciucci, *Prog. Mater. Sci.* **2021**, *116*, 100717.
[111] A. R. Puente Santiago, T. He, O. Eraso, M. A. Ahsan, A. N. Nair, V. S. Chava, T. Zheng, S. Pilla, O. Fernandez-Delgado, A. Du, *J. Am. Chem. Soc.* **2020**, *142*, 17923.
[112] P. Babar, A. Lokhande, H. H. Shin, B. Pawar, M. G. Gang, S. Pawar, J. H. Kim, *Small* **2018**, *14*, 1702568.
[113] A. R. Puente Santiago, O. Fernandez-Delgado, A. Gomez, M. A. Ahsan, L. Echegoyen, *Angew. Chem., Int. Ed.* **2021**, *133*, 124.
[114] J. Yang, W. Li, D. Wang, Y. Li, *Adv. Mater.* **2020**, *32*, 2003300.
[115] J. Chen, H. Li, C. Fan, Q. Meng, Y. Tang, X. Qiu, G. Fu, T. Ma, *Adv. Mater.* **2020**, *32*, 2003134.
[116] D. Bethune, R. Johnson, J. Salem, *Nature* **1993**, *366*, 123.
[117] R. B. Ross, C. M. Cardona, D. M. Guldi, S. G. Sankaranarayanan, M. O. Reese, N. Kopidakis, J. Peet, B. Walker, G. C. Bazan, E. Van Keuren, *Nat. Mater.* **2009**, *8*, 208.
[118] E. Pajootan, S. Omanovic, S. Coulombe, *Chem. Eng. J.* **2021**, *426*, 131706.
[119] J. Liang, Y. Liu, R. Liu, S. Zheng, Z. Si, D. Weng, F. Kang, *Nano Sel.* **2021**.
[120] J. Ji, Y. Zhang, L. Tang, C. Liu, X. Gao, M. Sun, J. Zheng, M. Ling, C. Liang, Z. Lin, *Nano Energy* **2019**, *63*, 103849.
[121] E. Yoo, T. Okata, T. Akita, M. Kohyama, J. Nakamura, I. Honma, *Nano Lett.* **2009**, *9*, 2255.
[122] M. Hong, J. Nie, X. Zhang, P. Zhang, Q. Meng, J. Huang, Z. Xu, C. Du, J. Chen, *J. Mater. Chem. A* **2019**, *7*, 25557.
[123] X. Wu, B. Feng, W. Li, Y. Niu, Y. Yu, S. Lu, C. Zhong, P. Liu, Z. Tian, L. Chen, *Nano Energy* **2019**, *62*, 117.
[124] Z. Jin, P. Li, Y. Meng, Z. Fang, D. Xiao, G. Yu, *Nat. Catal.* **2021**, *4*, 615.
[125] T. Sun, W. Zang, H. Yan, J. Li, Z. Zhang, Y. Bu, W. Chen, J. Wang, J. Lu, C. Su, *ACS Catal.* **2021**, *11*, 4498.
[126] S. Kang, Y. K. Jeong, S. Mhin, J. H. Ryu, G. Ali, K. Lee, M. Akbar, K. Y. Chung, H. Han, K. M. Kim, *ACS Nano* **2021**, *15*, 4416.
[127] P. J. Heptonstall, R. J. Gross, *Nat. Energy* **2021**, *6*, 72.
[128] T. He, S. K. Matta, G. Will, A. Du, *Small Methods* **2019**, *3*, 1800419.
[129] T. He, C. Zhang, G. Will, A. Du, *Catal. Today* **2020**, *351*, 113.
[130] J. Yang, W.-H. Li, K. Xu, S. Tan, D. Wang, Y. Li, *Angew. Chem., Int. Ed.* **2022**.
[131] S. Li, X. Hao, A. Abudula, G. Guan, *J. Mater. Chem. A* **2019**, *7*, 18674.
[132] W. Zhang, W. Lai, R. Cao, *Chem. Rev.* **2017**, *117*, 3717.
[133] B. Lu, Q. Liu, S. Chen, *ACS Catal.* **2020**, *10*, 7584.
[134] J. Mei, T. He, J. Bai, D. Qi, A. Du, T. Liao, G. A. Ayoko, Y. Yamauchi, L. Sun, Z. Sun, *Adv. Mater.* **2021**, *33*, 2104638.
[135] R. Li, D. Wang, *Adv. Energy Mater.* **2022**, *12*, 2103564.
[136] L. Zhang, K. Doyle-Davis, X. Sun, *Energy Environ. Sci.* **2019**, *12*, 492.
[137] B. Zandkarimi, A. N. Alexandrova, *J. Phys. Chem. Lett.* **2019**, *10*, 460.
[138] Q. Zhang, J. Guan, *Adv. Funct. Mater.* **2020**, *30*, 2000768.
[139] H. Zhang, X. F. Lu, Z.-P. Wu, X. W. D. Lou, *ACS Cent. Sci.* **2020**, *6*, 1288.
[140] L. Bai, C.-S. Hsu, D. T. Alexander, H. M. Chen, X. Hu, *Nat. Energy* **2021**, *6*, 1054.
[141] N. Wang, X. Chen, J. Jin, P. Zhang, X. Qiao, L. Cui, *Carbon* **2020**, *169*, 82.
[142] S. Chu, Y. Cui, N. Liu, *Nat. Mater.* **2017**, *16*, 16.
[143] S. Zhang, Q. Fan, R. Xia, T. J. Meyer, *Acc. Chem. Res.* **2020**, *53*, 255.
[144] B. Zhang, Y. Jiang, M. Gao, T. Ma, W. Sun, H. Pan, *Nano Energy* **2021**, *80*, 105504.
[145] Y. Pang, C. Su, G. Jia, L. Xu, Z. Shao, *Chem. Soc. Rev.* **2021**, *50*, 12744.
[146] C. Jia, K. Dastafkan, C. Zhao, *Curr. Opin. Electrochem.* **2022**, *31*, 100854.
[147] Y. Guo, S. Yao, Y. Xue, X. Hu, H. Cui, Z. Zhou, *Appl. Catal. B* **2022**, *304*, 120997.
[148] Y. Kong, T. He, A. R. Puente Santiago, D. Liu, A. Du, S. Wang, H. Pan, *ChemSusChem* **2021**, *14*, 3257.
[149] X. Mao, G. Kour, L. Zhang, T. He, S. Wang, C. Yan, Z. Zhu, A. Du, *Catal. Sci. Technol.* **2019**, *9*, 6800.
[150] K. Jiang, S. Siahrostami, T. Zheng, Y. Hu, S. Hwang, E. Stavitski, Y. Peng, J. Dynes, M. Gangisetty, D. Su, *Energy Environ. Sci.* **2018**, *11*, 893.
[151] W. Zang, T. Yang, H. Zou, S. Xi, H. Zhang, X. Liu, Z. Kou, Y. Du, Y. P. Feng, L. Shen, *ACS Catal.* **2019**, *9*, 10166.
[152] T. Ding, X. Liu, Z. Tao, T. Liu, T. Chen, W. Zhang, X. Shen, D. Liu, S. Wang, B. Pang, *J. Am. Chem. Soc.* **2021**, *143*, 11317.
[153] M. I. Ahmed, S. Chen, W. Ren, X. Chen, C. Zhao, *Chem. Commun.* **2019**, *55*, 12184.
[154] H. Jing, P. Zhu, X. Zheng, Z. Zhang, D. Wang, Y. Li, *Adv. Powder Mater.* **2021**, *1*, 100013.
[155] T. He, L. Zhang, G. Kour, A. Du, *J. CO2 Util.* **2020**, *37*, 272.
[156] X. Bai, Q. Li, L. Shi, X. Niu, C. Ling, J. Wang, *Small* **2020**, *16*, 1901981.
[157] S. Chen, J. Bie, W. Fa, Y. Zha, Y. Gao, X. C. Zeng, *ACS Appl. Nano Mater.* **2018**, *2*, 535.
[158] H. Zhang, J. Li, S. Xi, Y. Du, X. Hai, J. Wang, H. Xu, G. Wu, J. Zhang, J. Lu, *Angew. Chem., Int. Ed.* **2019**, *131*, 15013.
[159] X. Liu, Y. Jiao, Y. Zheng, M. Jaroniec, S.-Z. Qiao, *J. Am. Chem. Soc.* **2019**, *141*, 9664.
[160] L. Li, C. Tang, H. Jin, K. Davey, S.-Z. Qiao, *Chem* **2021**, *7*, 3232.
[161] L. Zhang, J. M. T. A. Fischer, Y. Jia, X. Yan, W. Xu, X. Wang, J. Chen, D. Yang, H. Liu, L. Zhuang, *J. Am. Chem. Soc.* **2018**, *140*, 10757.
[162] X. Liu, Y. Jiao, Y. Zheng, S.-Z. Qiao, *ACS Catal.* **2020**, *10*, 1847.
[163] S. Tian, B. Wang, W. Gong, Z. He, Q. Xu, W. Chen, Q. Zhang, Y. Zhu, J. Yang, Q. Fu, *Nat. Commun.* **2021**, *12*, 1.
[164] Z. Chen, L. Chen, C. Yang, Q. Jiang, *J. Mater. Chem. A* **2019**, *7*, 3492.
[165] T. Cui, Y.-P. Wang, T. Ye, J. Wu, Z. Chen, J. Li, Y. Lei, D. Wang, Y. Li, *Angew. Chem., Int. Ed.* **2022**, *61*, e202115219.
[166] C. R. Rêgo, P. Tereshchuk, L. N. Oliveira, J. L. Da Silva, *Phys. Rev. B* **2017**, *95*, 235422.
[167] C. Ling, X. Niu, Q. Li, A. Du, J. Wang, *J. Am. Chem. Soc.* **2018**, *140*, 14161.
[168] Q. Li, X. Bai, C. Ling, Q. Zhou, S. Yuan, Q. Chen, J. Wang, *Small Methods* **2019**, *3*, 1800315.
[169] M. Ha, D. Y. Kim, M. Umer, V. Gladkikh, C. W. Myung, K. S. Kim, *Energy Environ. Sci.* **2021**, *14*, 3455.
[170] F. R. Fan, R. Wang, H. Zhang, W. Wu, *Chem. Soc. Rev.* **2021**, *50*, 10983.
[171] D. Gao, T. Liu, G. Wang, X. Bao, *ACS Energy Lett.* **2021**, *6*, 713.
[172] A. Pedersen, J. Barrio, A. Li, R. Jervis, D. J. Brett, M. M. Titirici, I. E. Stephens, *Adv. Energy Mater.* **2021**, *12*, 2102715.
[173] J. Xu, A. Elangovan, J. Li, B. Liu, *J. Phys. Chem. C* **2021**, *125*, 2334.
[174] T. He, C. Zhang, A. Du, *Chem. Eng. Sci.* **2019**, *194*, 58.
[175] Y. Li, H. Su, S. H. Chan, Q. Sun, *ACS Catal.* **2015**, *5*, 6658.
[176] T. He, S. K. Matta, A. Du, *Phys. Chem. Chem. Phys.* **2019**, *21*, 1546.
[177] J. Li, X. Gao, L. Zhu, M. N. Ghazzal, J. Zhang, C.-H. Tung, L.-Z. Wu, *Energy Environ. Sci.* **2020**, *13*, 1326.
[178] Z.-Z. Lin, *Carbon* **2016**, *108*, 343.
[179] T. He, K. Reuter, A. Du, *J. Mater. Chem. A* **2020**, *8*, 599.
[180] G. Gao, Y. Jiao, E. R. Waclawik, A. Du, *J. Am. Chem. Soc.* **2016**, *138*, 6292.
[181] X. Li, W. Zhong, P. Cui, J. Li, J. Jiang, *J. Phys. Chem. Lett.* **2016**, *7*, 1750.
[182] F. Li, X. Liu, Z. Chen, *Small Methods* **2019**, *3*, 1800480.

[183] X. Lv, W. Wei, B. Huang, Y. Dai, T. Frauenheim, *Nano Lett.* **2021**, *21*, 1871.
[184] T. He, G. Kour, X. Mao, A. Du, *J. Catal.* **2020**, *382*, 49.
[185] X. Wang, Y. Zhang, J. Wu, Z. Zhang, Q. Liao, Z. Kang, Y. Zhang, *Chem. Rev.* **2021**, *122*, 1273.
[186] H. Li, Y. Liu, K. Chen, J. T. Margraf, Y. Li, K. Reuter, *ACS Catal.* **2021**, *11*, 7906.
[187] C. Ling, Y. Ouyang, Q. Li, X. Bai, X. Mao, A. Du, J. Wang, *Small Methods* **2019**, *3*, 1800376.
[188] C. Ling, X. Bai, Y. Ouyang, A. Du, J. Wang, *J. Phys. Chem. C* **2018**, *122*, 16842.
[189] J. Chang, G. Wang, M. Wang, Q. Wang, B. Li, H. Zhou, Y. Zhu, W. Zhang, M. Omer, N. Orlovskaya, *Nat. Energy* **2021**, *6*, 1144.
[190] L. Li, S. Huang, R. Cao, K. Yuan, C. Lu, B. Huang, X. Tang, T. Hu, X. Zhuang, Y. Chen, *Small* **2021**, *18*, 2105387.
[191] H. Li, J. Xiao, Q. Fu, X. Bao, *Proc. Natl. Acad. Sci. USA* **2017**, *114*, 5930.
[192] J. Xiao, X. Pan, S. Guo, P. Ren, X. Bao, *J. Am. Chem. Soc.* **2015**, *137*, 477.
[193] S. Zhou, X. Yang, X. Xu, S. X. Dou, Y. Du, J. Zhao, *J. Am. Chem. Soc.* **2019**, *142*, 308.
[194] Q. Fu, X. Bao, *Nat. Catal.* **2019**, *2*, 834.
[195] T. He, G. Gao, L. Kou, G. Will, A. Du, *J. Catal.* **2017**, *354*, 231.
[196] C. Zhang, L. Kou, T. He, Y. Jiao, T. Liao, S. Bottle, A. Du, *Comput. Mater. Sci.* **2018**, *149*, 158.
[197] G. Gao, Y. Jiao, F. Ma, Y. Jiao, E. Waclawik, A. Du, *J. Catal.* **2015**, *332*, 149.
[198] W. Liu, Y. Kong, B. Wang, X. Li, P. Liu, A. R. P. Santiago, T. He, *Nanomaterials* **2021**, *11*, 3173.
[199] Z. Zhang, X. Zhao, S. Xi, L. Zhang, Z. Chen, Z. Zeng, M. Huang, H. Yang, B. Liu, S. J. Pennycook, *Adv. Energy Mater.* **2020**, *10*, 2002896.
[200] Y. Pan, S. Liu, K. Sun, X. Chen, B. Wang, K. Wu, X. Cao, W. C. Cheong, R. Shen, A. Han, *Angew. Chem., Int. Ed.* **2018**, *57*, 8614.
[201] X. Xie, L. Shang, X. Xiong, R. Shi, T. Zhang, *Adv. Energy Mater.* **2021**, *12*, 2102688.
[202] Y. Tan, W. Zhu, Z. Zhang, W. Wu, R. Chen, S. Mu, H. Lv, N. Cheng, *Nano Energy* **2021**, *83*, 105813.
[203] X. Xie, L. Shang, X. Xiong, R. Shi, T. Zhang, *Adv. Energy Mater.* **2022**, *12*, 2102688.
[204] S. Matsuda, Y. Niitsuma, Y. Yoshida, M. Umeda, *Sci. Rep.* **2021**, *11*, 1.
[205] T. Qu, J. Hu, X. Dai, Q. Tan, Y. Liu, Y. Chen, S. Guo, Y. Liu, *ACS Appl. Mater. Interfaces* **2021**, *13*, 23523.
[206] H. Gul, W. Raza, J. Lee, M. Azam, M. Ashraf, K.-H. Kim, *Chemosphere* **2021**, *281*, 130828.
[207] I. Gajda, J. Greenman, I. A. Ieropoulos, *Curr. Opin. Electrochem.* **2018**, *11*, 78.
[208] X. Zhang, X. Guo, Q. Wang, R. Zhang, T. Xu, P. Liang, X. Huang, *J. Mater. Chem. A* **2020**, *8*, 10772.
[209] J. Wang, Z. Huang, W. Liu, C. Chang, H. Tang, Z. Li, W. Chen, C. Jia, T. Yao, S. Wei, *J. Am. Chem. Soc.* **2017**, *139*, 17281.

Tianwei He received his Ph.D. degree in Physical Chemistry in 2020 from the Queensland University of Technology, Australia. He is currently working as a postdoctoral researcher at the Fritz Haber Institute of the Max Planck Society in Berlin, Germany. He has published over 30 articles in very prestigious journals such as *Journal of the American Chemical Society*, *Advanced Materials*, *Small Methods*, *Small*, *Journal of Materials Chemistry A*, and *Nano Research*. His research interest mainly focuses on computational discovery and design catalysts that are active, efficient, selective, stable, and cheap that can ultimately enable large-scale applications.

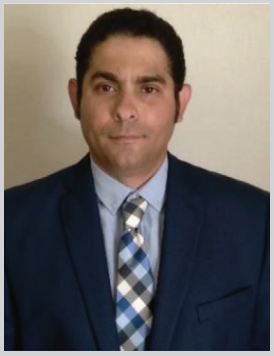

Alain R. Puente Santiago received his Ph.D. degree in Physical Chemistry with distinction (July 2017) from the University of Cordoba, Spain. He is currently working as a research fellow in Prof. Goodenough's group at the University of Texas at Austin. He has published 60 articles in very prestigious journals such as *Journal of the American Chemical Society*, *Angewandte Chemie*, *Journal of Materials Chemistry A*, *ACS Applied Materials, and Interfaces*, *Journal of Catalysis*, *Chemical Society Reviews A*, and *Green Chemistry*. His research interests tackle the development of low-dimensional nanostructures for electrocatalytic, sensing, and energy storage applications.

Shiyu Xia is currently pursuing her Ph.D. degree under the guidance of Prof. Guobao Xu at Changchun Institute of Applied Chemistry (CIAC) in the Chinese Academy of Sciences (CAS). She received her B.Sc. degree from Zhengzhou University in 2019. Her present research interests mainly focus on the controllable synthesis of noble metal nanocrystals for electrocatalysis and nanozyme.

Md Ariful Ahsan received his Ph.D. in Chemistry from the University of Texas at El Paso in 2021, under the supervision of Prof. Juan C. Noveron. Currently, he is working as a postdoctoral scientist with Prof. John B. Goodenough at UT Austin. He has published over 45 articles in peer-reviewed prestigious journals, including *Journal of the American Chemical Society*, *Angewandte Chemie*, *Green Chemistry*, and *Communications Materials*. His research focuses on multi-functional nanomaterials for electrochemical sensing, wastewater treatment, and clean energy conversion technologies.

Guobao Xu received B.Sc. from Jilin University, M.Sc. from Xiamen University, and Ph.D. from CIAC. After postdoctoral research at the University of Hong Kong, Hong Kong Polytechnic University, and JST-NTT, he joined CIAC in 2004. He was chairperson of the Organization Committee of 15–18th International Symposium on Electroanalytical Chemistry and The Third International Meeting on Electrogenerated Chemiluminescence. The research interests of his group include electrochemistry, nanostructure synthesis, biosensor, and devices.

Rafael Luque (Ph.D. in 2005 from Universidad de Cordoba, Spain) has significant experience in biomass and waste valorization practices to materials, fuels, and chemicals as well as nanoscale chemistry (600+ publications, h-index 89, 34 000 citations, 7 patents, more than 10 edited books). Prof. Luque is editor-in-chief of *Molecular Catalysis* and is serving on the Advisory/Editorial Board of more than 10 Q1 RSC, Wiley, ACS, and Elsevier journals. Prof. Luque was named 2018, 2019, 2020, and 2021 Highly Cited Researcher (Clarivate Analytics).